Rim2α determines docking and priming states in insulin granule exocytosis

Yasuda, Takao

(Degree)
博士（医学）

(Date of Degree)
2010-09-25

(Date of Publication)
2011-03-03

(Resource Type)
doctoral thesis

(Report Number)
甲5051

(URL)
https://hdl.handle.net/20.500.14094/D1005051

Rim2α determines docking and priming states in insulin granule exocytosis

Rim2αはインスリン顆粒開口分泌における ドッキングとプライミング状態を決定づける

安田　貴雄、柴崎 忠雄、南　幸太郎、高橋　晴美、溝口　明、瓜生　幸嗣、
沼田　朋大、森　泰生、宮崎　純一、三木　隆司、清野　進

神戸大学大学院医学系研究科医科学専攻
細胞分子医学
(指導教員：清野　進　教授)

安田　貴雄

Key words: Rim2α, Rab3A, Munc13-1, Epac2, Docking, Priming

Title: Rim2α determines docking and priming states in insulin granule exocytosis

Running Title: Role of Rim2α in insulin granule exocytosis

Authors/Affiliations

Takao Yasuda,[1] Tadao Shibasaki,[1] Kohtaro Minami,[1] Harumi Takahashi,[1] Akira Mizoguchi,[3] Yoshitsugu Uriu,[4] Tomohiro Numata,[4] Yasuo Mori,[4] Jun-ichi Miyazaki,[5] Takashi Miki,[1,6] and Susumu Seino[1,2,7]

[1]Division of Cellular and Molecular Medicine, Department of Physiology and Cell Biology and [2]Division of Diabetes and Endocrinology, Department of Internal Medicine, Kobe University Graduate School of Medicine, Kobe, Hyogo, 650-0017, Japan.

[3]Department of Neural Regeneration and Cell Communication, Mie University Graduate School of Medicine, Tsu, Mie 514-8507, Japan

[4]Department of Synthetic Chemistry and Biological Chemistry, Graduate School of Engineering, Kyoto University, Kyoto 615-8510, Japan

[5]Division of Stem Cell Regulation Research, Osaka University Graduate School of Medicine, 2-2 Yamadaoka, Suita, Osaka 565-0871, Japan

[6]Department of Autonomic Physiology, Graduate School of Medicine, Chiba University, 1-8-1, Inohana, Chuo-ku, Chiba, 260-8670, Japan

[7]Core Research for Evolutional Science and Technology (CREST), Japan Science and Technology Agency, 4-1-8, Hon-cho, Kawaguchi, Saitama 332-0012, Japan

Contact

E-mail: seino@med.kobe-u.ac.jp Tel: +81-78-382-5860 Fax: +81-78-382-6762

Summary

Insulin secretion is essential for maintenance of glucose homeostasis, but the mechanism of insulin granule exocytosis, the final step of insulin secretion, is largely unknown. Here we investigated the role of Rim2α in insulin granule exocytosis including the docking, priming, and fusion steps. We found that interaction of Rim2α and Rab3A is required for docking, which is considered a brake on fusion events, and that docking is necessary for K^+-induced exocytosis but not for glucose-induced exocytosis. Furthermore, we found that dissociation of the Rim2α/Munc13-1 complex by glucose stimulation activates Syntaxin1 by Munc13-1, indicating that Rim2α primes insulin granules for fusion. Thus, Rim2α determines docking and priming states in insulin granule exocytosis depending on its interacting partner, Rab3A or Munc13-1, respectively. Since Rim2α$^{-/-}$ mice exhibit impaired secretion of various hormones stored as dense-core granules, including glucose-dependent insulinotropic polypeptide, growth hormone, and epinephrine, Rim2α plays a critical role in exocytosis of dense-core granules.

Introduction

Stimulus-secretion coupling has been characterized in neurons and neuroendocrine and endocrine cells (Burgoyne and Morgan, 2003; Sudhof, 2004; Seino and Shibasaki, 2005). Pancreatic β-cells, in which insulin is stored as dense-core vesicles, play a central role in glucose homeostasis. Although understanding of the molecular mechanisms of cell signaling in insulin secretion has deepened remarkably in recent years, the mechanisms of insulin granule exocytosis, the final step in the insulin secretory process, are largely unknown.

Recently, various molecules interacting with the insulin granules have been identified (Brunner et al., 2007), including Rab27A (Kasai et al., 2005), granuphilin (Gomi et al., 2005), ZnT8 (Nicolson et al., 2009), Noc2 (Matsumoto et al., 2004), collectrin (Fukui et al., 2005), and Rap1 (Shibasaki et al., 2007). Mutation of the Rab27A gene was discovered from Griscelli syndrome in human characterized by hypopigmentation and loss of cytotoxic killing activity by cytotoxic T lymphocytes

(Menasche et al., 2000). The same mutation found in the mouse coat-color mutant *ashen* causes a defect in insulin granule exocytosis (Kasai et al., 2005). Granuphilin$^{-/-}$ mice, ZnT8$^{-/-}$ mice, Noc2$^{-/-}$ mice, and transgenic mice overexpressing collectrin also exhibit impaired insulin secretion and abnormal glucose homeostasis.

We previously identified Rab3-interacting molecule 2 (Rim2) by yeast two-hybrid screen of a clonal pancreatic β-cell (MIN6) cDNA library (Ozaki et al., 2000). Rim2 is now known as a multidomain protein that occurs as three variants including Rim2α, Rim2β, and Rim2γ (Wang and Sudhof, 2003). Rim2α, the full-length form of Rim2, is composed of an N-terminal Zn^{2+}-finger domain, a central PDZ and C_2A domains, and a C-terminal C_2B domain. Rim2β lacks the N-terminal Zn^{2+}-finger domain of Rim2α, while Rim2γ is composed only of the C-terminal C_2B domain of Rim2α with flanking sequences. Rim2α interacts with Rab3A (Ozaki et al., 2000), Munc13-1 (Dulubova et al., 2005), and Rab8 (Fukuda, 2003) at the N-terminal region. In addition to interaction with these proteins, Rim2α binds to cAMP-GEFII (also referred to as Epac2) (Ozaki et al., 2000; Shibasaki et al., 2004) and ELKS (Ohara-Imaizumi et al., 2005; Inoue et al., 2006) through the central PDZ domain, to Piccolo through a C_2A domain (Fujimoto et al., 2002), to RIM-BPs through a PXXP sequence between the two C_2-domains (Hibino et al., 2002), and to Liprin-α1 and synaptotagmin 1 through the C-terminal C_2B domain (Schoch et al., 2002). These findings suggest that Rim2α functions as a scaffold protein and that it is involved in regulated exocytosis. Indeed, Rim2α has been found to be involved in cAMP-potentiated insulin secretion through the Epac2 pathway in *in vitro* studies (Ozaki et al., 2000; Kashima et al., 2001). Although Rim2α is expressed mainly in endocrine and neuroendocrine cells such as pancreatic β-cells, pituitary, and adrenal gland, it is unknown how Rim2α acts in the steps in the process of exocytosis including recruitment, docking, priming, and fusion.

Rim1α, an isoform of Rim2α, is expressed mainly in brain and a putative Rab3 effector involved in the regulation of synaptic vesicle fusion (Wang et al., 1997). Studies of Rim1α$^{-/-}$ mice (Castillo et al., 2002; Lonart et al., 2003) and the null mutation of Rim in *C. elegans* (Koushika et al., 2001)

indicate that Rim1α is important for long-term potentiation by increasing neurotransmitter release at mossy-fiber synapses in the CA3 region in hippocampus of cerebrum and that it is involved in a post-docking step. To clarify the role of Rim2α in endocrine function both *in vitro* and *in vivo*, we generated Rim2α$^{-/-}$ mice. In the course of our study, Schoch et al also generated Rim2α$^{-/-}$ mice and reported the phenotype of the mice (Schoch et al., 2006). They found no apparent developmental abnormalities of these mice, but there were slight behavioral differences and slightly lower survival rates compared to Rim2α$^{+/+}$ mice. They also found no changes in body fat content or blood glucose levels in Rim2α$^{-/-}$ mice. However, no study of endocrine or neuroendocrine functions in Rim2α$^{-/-}$ mice was reported.

In the present study, we show that Rim2α is required for the docking and priming states in insulin granule exocytosis through interaction with Rab3A and Munc13-1, respectively, and that although docking is necessary for K^+-induced exocytosis, it is unnecessary for glucose-induced exocytosis. In addition, we found secretory defects in various hormones including glucose-dependent insulinotropic polypeptide (GIP), growth hormone (GH), and epinephrine in Rim2α$^{-/-}$ mice *in vivo*. Thus, Rim2α is a key molecule in insulin granule exocytosis and also is required in normal secretion of hormones associated with glucose homeostasis.

Results

Insulin and GIP secretion are impaired in Rim2α$^{-/-}$ mice *in vivo*

The Rim2 gene has three independent promoters that create three variant forms of Rim2, Rim2α, Rim2β, and Rim2γ (Wang and Sudhof, 2003) (Figure S1A). We found that among the three variants Rim2α is predominantly expressed in pancreatic islets and insulin secreting MIN6 cells (Figure S1B and S1C). We generated Rim2α$^{-/-}$ mice in which the fourth exon of the Rim2 gene was replaced by Neo cassette (Figure S1D). The absence of Rim2α expression in Rim2α$^{-/-}$ mice was confirmed by northern blot analysis, reverse transcription PCR, and immunoblot analysis (Figure S1E-S1G). The expression levels of Rim2β and Rim2γ were not changed in Rim2α$^{-/-}$ mice (Figure S1H). Rim2α$^{-/-}$

mice were viable and fertile. Rim2α$^{-/-}$ mice exhibited islet hyperplasia (Rim2α$^{+/+}$ = 7,887.6 ± 728.1 μm^2; Rim2α$^{-/-}$ = 15,620.4 ± 1486.7 μm^2; *N*=4 and 100 islets; $p < 0.01$) and a relatively increased number of α-cells (Rim2α$^{+/+}$ = 14.7 ± 1.5% of islets; Rim2α$^{-/-}$ = 40.0 ± 2.5% of islets; $p < 0.01$; *N*=3, n=53 for Rim2α$^{+/+}$ and n=37 for Rim2α$^{-/-}$) (Figure S1I).

We performed intraperitoneal glucose tolerance test (IPGTT) to examine pancreatic endocrine function in Rim2α$^{-/-}$ mice. The fasting blood glucose levels of Rim2α$^{-/-}$ mice were significantly decreased compared those of Rim2α$^{+/+}$ mice (Rim2α$^{+/+}$ = 119 ± 3.1 mg/dl; Rim2α$^{-/-}$ = 87 ± 4.7 mg/dl; $p < 0.01$; n=19 for Rim2α$^{+/+}$ and n=17 for Rim2α$^{-/-}$). The blood glucose levels of Rim2α$^{-/-}$ mice 60 min after intraperitoneal glucose administration were significantly higher than those of Rim2α$^{+/+}$ mice. The insulin response during IPGTT in Rim2α$^{-/-}$ mice was markedly lower than that in Rim2α$^{+/+}$ mice (Figure 1A). We also examined changes in blood glucose and insulin levels after oral glucose administration (OGTT). The blood glucose levels of Rim2α$^{-/-}$ mice during OGTT were significantly higher than those of Rim2α$^{+/+}$ mice at all time points examined. The insulin levels were markedly reduced in Rim2α$^{-/-}$ mice compared to those in Rim2α$^{+/+}$ mice (Figure 1B). Similar results were obtained by oral mixed meal administration (Figure 1C). These results suggest that incretin secretion is decreased in Rim2α$^{-/-}$ mice. GIP, an incretin secreted by enteroendocrine cells in response to ingestion of nutrients, potentiates glucose-induced insulin secretion (Drucker, 2006). To investigate the possible involvement of incretins in this reduced insulin secretion, we attempted to measure the serum levels of GIP and glucagon-like peptide-1 (GLP-1) in Rim2α$^{-/-}$ mice. Although GIP-secreting K cells were present in Rim2α$^{-/-}$ mice (Figure S1J), serum GIP levels in Rim2α$^{-/-}$ mice were below the sensitivity of assay (Figure 1D). However, the measurement of GLP-1, another incretin, in mouse serum was not possible by using commercially available kits despite several attempts. These results indicate that both insulin and GIP secretion in Rim2α$^{-/-}$ mice are markedly impaired.

Insulin secretion is impaired in pancreatic islets of Rim2α$^{-/-}$ mice

As shown in Figure 2A, insulin content of the islets of Rim2α$^{-/-}$ mice was increased 1.4 fold, compared to that of Rim2α$^{+/+}$ mice. Both glucose-induced and Ca^{2+}-triggered insulin secretion (assessed by 60 mM K^+ stimulation) from pancreatic islets of Rim2α$^{-/-}$ mice were significantly decreased, compared to those from pancreatic islets of Rim2α$^{+/+}$ mice (Figure 2B). We then examined insulin secretion potentiated by cAMP in pancreatic islets of Rim2α$^{-/-}$ mice. GIP-potentiated insulin secretion from pancreatic islets of Rim2α$^{-/-}$ mice was significantly lower than that of Rim2α$^{+/+}$ mice (Figure 2C). The cAMP analog 8-Bromo-cAMP-potentiated insulin secretion also was significantly reduced in pancreatic islets of Rim2α$^{-/-}$ mice. These results strongly suggest that Rim2α plays a major role in insulin secretion.

The number of docked insulin granules is decreased in pancreatic β-cells of Rim2α$^{-/-}$ mice

We investigated the role of Rim2α in insulin granule exocytosis. For this purpose, we analyzed the dynamics of insulin granules in living pancreatic β-cells using total internal reflection fluorescence microscopy (TIRFM) (Shibasaki et al., 2007). We confirmed that the modes of insulin granule exocytosis can be classified into three groups depending on the dynamics of the insulin granules: 1) fusion events involving granules that are predocked to the plasma membrane (*old face*); 2) fusion events involving granules that are newly recruited and immediately fused to the plasma membrane without docking (*restless newcomer*); and 3) fusion events involving granules that are newly recruited, docked, and then fused to the plasma membrane (*resting newcomer*).

As shown in Figure 3A, the number of docked insulin granules in pancreatic β-cells of Rim2α$^{-/-}$ mice was markedly decreased, compared to that in pancreatic β-cells of Rim2α$^{+/+}$ mice. We have previously shown that most K^+-induced fusion events involve *old face* (Shibasaki et al., 2007). As expected, the number of fusion events caused by K^+ stimulation in pancreatic β-cells of Rim2α$^{-/-}$ mice was significantly decreased due to the marked reduction in the number of *old face* (Figure 3B). In contrast, glucose-induced fusion events comprised mainly *restless newcomer*. Fusion events, mainly in the first phase, were markedly decreased in pancreatic β-cells of Rim2α$^{-/-}$ mice, and those

in the second phase were also decreased (Figure 3C). *Resting newcomer*, which docks to the plasma membrane before fusion, were not detected in pancreatic β-cells of Rim2α$^{-/-}$ mice. These results indicate that Rim2α is required in normal regulation of insulin granule exocytosis.

The defect in insulin granule exocytosis in Rim2α$^{-/-}$ mice is not due to changes in expression or distribution of exocytosis-associated proteins

We intended to examine the expression and subcellular localization of exocytosis-associated proteins as a consequence of Rim2α deficiency, using pancreatic β-cells of Rim2α$^{-/-}$ mice. However, the limited number of isolated pancreatic β-cells of these mice made such an experiment impossible. We therefore established clonal pancreatic β-cells lacking Rim2α (Rim2α$^{ko/ko}$ β-cells) by crossbreeding Rim2α$^{-/-}$ mice and *IT6* mice expressing simian virus 40 large T antigen under human insulin promoter (Miyazaki et al., 1990). The absence of Rim2α expression in Rim2α$^{ko/ko}$ β-cells was confirmed by immunocytochemical and immunoblot analyses using anti-Rim2 antibody (Figure 4A and 4B).

To determine whether deficiency of Rim2α affects the expression levels and localization of exocytosis-associated proteins, we compared those of the proteins in MIN6 cells and Rim2α$^{ko/ko}$ β-cells. We found no significant differences in the expression levels of any of the proteins examined (Figure 4B). The expression levels did not differ in Rim2α$^{ko/ko}$ β-cells expressing wild-type (WT) Rim2α by adenovirus-mediated gene transfer. We examined localization of Rim2α and exocytosis-associated proteins in MIN6 cells by immunostaining and subcellular fractionation experiments. Rim2α was localized on both insulin granules and plasma membrane (Figure 4A and 4C), whereas Rab3A, Munc13-1, and Syntaxin1 were localized on the plasma membrane (Figure 4C). The localizations of these proteins were the same in Rim2α$^{ko/ko}$ β-cells.

We then examined insulin secretion in Rim2α$^{ko/ko}$ β-cells. Both glucose- and K^+-induced insulin secretion from Rim2α$^{ko/ko}$ β-cells were significantly reduced, compared to those from MIN6 cells (Figure 4D). Similarly to the pancreatic β-cells of Rim2α$^{-/-}$ mice, the number of docked insulin

granules was significantly decreased in Rim2α$^{ko/ko}$ β-cells (Figure 4E). Importantly, the defects in both insulin secretion and the number of docked insulin granules were rescued when WT Rim2α was exogenously introduced by adenovirus-based gene transfer (Figure 4D and 4E). These results indicate that Rim2α is required for the docking step in insulin granule exocytosis.

Rim2α, Rab3A, and Munc13-1 form a complex regulated by glucose

Because the expression levels and localization of exocytosis-associated proteins in Rim2α$^{ko/ko}$ β-cells did not differ from those in MIN6 cells, we explored the possibility that the interaction of Rim2α and Rim2α-binding proteins is critical for regulated exocytosis of insulin granules. We performed immunoprecipitation experiments on the interaction of Rim2α with Rab3A or Munc13-1 by glucose stimulation. The interaction of Rim2α and Munc13-1 was decreased by glucose stimulation (Figure 4F and Figure S2). However, no interaction of Rim2α and endogenous Rab3A was detected (Figure 4F). This suggests that most of the endogenous Rab3A is likely to be in the GDP-inactivated state since Rim2α binds to the GTP-activated form of Rab3A (Ozaki et al., 2000). In fact, we found that Rim2α interacted with the GTP-activated form of Rab3A (Figure 4F). Therefore, we examined the effect of the active form of Rab3A on the interaction of Rim2α and Munc13-1. The interaction of Rim2α and Munc13-1 in the presence of the constitutively active form of Rab3A (Q81L) (Brondyk et al., 1993) was detected in a glucose concentration-independent manner (Figure 4F and Figure S2). These results indicate that Munc13-1 dissociates from the Rim2α/Munc13-1 complex by glucose stimulation.

Rim2α is critical for docking and priming of insulin granules

The finding of differences in the interactions with these three molecules indicates that Rim2α is involved in the recruitment, docking, and/or priming steps. Rab3A and Munc13-1 have been shown to interact with the N-terminal region of Rim2α (Dulubova et al., 2005). To determine whether the impaired insulin secretion in Rim2α$^{ko/ko}$ β-cells is caused by defective interaction of Rim2α with

Rab3A, Munc13-1, or both of them, we prepared a double mutant (E36A/R37S) of Rim2α that cannot bind to Rab3A but can bind to Munc13-1 (Fukuda, 2004). Using this mutant, we examined insulin secretion and the number of docked insulin granules in Rim2α$^{ko/ko}$ β-cells. Although the mutant Rim2α (E36A/R37S) was able to restore both glucose- and K^+-induced insulin secretion (Figure 5A upper left panel and Figure 6A), the mutant Rim2α (E36A/R37S) was unable to restore the number of docked insulin granules (Figure 5A upper right panel), suggesting that the interaction of Rim2α and Rab3A is required for docking of the insulin granules but not for fusion of the granules to the plasma membrane. Interestingly, because K^+-induced insulin secretion in Rim2α$^{ko/ko}$ β-cells was significantly higher than that by WT Rim2α gene transfer, the interaction of Rim2α and Rab3A may negatively regulate insulin secretion (Figure 5A upper panels, lower left panel and Figure 6A), that is, docking may be a state preventing fusion (i.e., a braking state).

We then prepared a double mutant (K136E/K138E) of Rim2α that cannot bind to Munc13-1 but can bind to Rab3A (Dulubova et al., 2005). Although the mutant Rim2α (K136E/K138E) was unable to restore either glucose- or K^+-induced insulin secretion (Figure 5A, upper left panel and Figure 6A), the mutant was able to restore the number of docked insulin granules (Figure 5A, upper right panel). These results suggest that interaction of Rim2α and Munc13-1 after the docking step is required for insulin granule exocytosis (Figure 5A, upper panels, lower right panel and Figure 6A).

To examine whether Rim2α enhances Munc13-1 activity in pancreatic β-cells, we evaluated insulin secretion in Rim2α$^{ko/ko}$ β-cells by phorbol 12-myristate 13-acetate (PMA), which is known to enhance Munc13-1 activity in pancreatic β-cells (Betz et al., 1998; Kang et al., 2006). Glucose-induced insulin secretion was restored in Rim2α$^{ko/ko}$ β-cells in the presence of PMA (Figure 5B, left panel and Figure 6B). However, the number of docked insulin granules was not increased in Rim2α$^{ko/ko}$ β-cells (Figure 5B, middle panel). These results suggest that Rim2α directly activates Munc13-1 and that it regulates post-docking steps of insulin granule exocytosis (Figure 5B, right panel).

Activation of Munc13-1 is proposed to change Syntaxin1 from the closed state to the open state,

initiating the priming step of granule exocytosis (Madison et al., 2005). Thus, Syntaxin1 might not be activated in Rim2α$^{ko/ko}$ β-cells. If that is the case, introduction of exogenous open Syntaxin1 into Rim2α$^{ko/ko}$ β-cells should bypass the interaction of Rim2α and Munc13-1 to stimulate insulin secretion directly. To investigate this possibility, we examined insulin secretion and the number of docked insulin granules in Rim2α$^{ko/ko}$ β-cells after gene transfer of open Syntaxin1 (Dulubova et al., 1999). Open Syntaxin1 fully restored both glucose- and K^+-induced insulin secretion, but WT Syntaxin1 did not restore it (Figure 5C left panel and Figure 6C). In contrast, both forms of Syntaxin1 were unable to restore the number of docked insulin granules (Figure 5C, middle panel). These findings indicate that interaction of Rim2α and Munc13-1 is required in the process of exocytosis between the docking and the fusion steps, suggesting that such interaction underlies priming of insulin granules.

Rim2α is required for Epac2-potentiated insulin secretion

Rim2α was originally identified as a molecule that interacts with Epac2 (Ozaki et al., 2000). Because Epac2 is responsible for cAMP-induced, PKA-independent exocytosis, interaction of Rim2α and Epac2 is thought to be involved in cAMP-potentiated insulin secretion (Ozaki et al., 2000; Kashima et al., 2001). To clarify the role of Rim2α in cAMP-potentiated insulin secretion, we utilized Rim2α$^{ko/ko}$ β-cells, preparing a triple mutant (R682A, L688A, and G689A) (PDZ-AAA) of Rim2α that disrupts the interaction of Rim2α and Epac2 (Shibasaki et al., 2004). This mutant Rim2α (PDZ-AAA) significantly rescued, although not completely, glucose-induced insulin secretion. Importantly, the glucose-induced insulin secretion potentiated by the Epac specific cAMP analog 8-pCPT-2'-*O*-Me-cAMP-AM (Vliem et al., 2008) failed to potentiate insulin secretion in these cells (Figure 7). These results make clear that Rim2α mediates cAMP-induced, Epac2-dependent insulin secretion.

Rim2α deficiency causes multiple defects in hormone secretion

Systemic analysis of offspring from heterozygous mating revealed that Rim2α$^{-/-}$ mice were smaller than littermate Rim2α$^{+/+}$ mice (Figure S1K). Both basal and hypoglycemia-induced GH secretion were markedly reduced in Rim2α$^{-/-}$ mice (Figure S1L), and insulin-like growth factor-1 (IGF-1) levels were decreased in the mice (Figure S1M). In addition, hypoglycemia-induced epinephrine secretion was significantly decreased in Rim2α$^{-/-}$ mice (Figure S1N). In contrast, hypoglycemia-induced glucagon secretion was significantly increased in Rim2α$^{-/-}$ mice (Figure S1O), a finding consistent with the increase in the number of α-cells. Taken together, these results show that Rim2α is required for normal regulation of hormone secretion associated with glucose homeostasis.

Discussion

Rim1α is a multidomain adaptor protein that was discovered as a putative effector of Rab3 (Wang et al., 1997). The null mutation of Rim in *C. elegans* was shown to decrease the number of fusion-competent vesicles, suggesting a role in the post-docking process (Koushika et al., 2001). We previously identified Rim2α as a molecule interacting with Epac2, and found that it was required for cAMP-dependent, PKA-independent insulin secretion *in vitro* (Ozaki et al., 2000; Kashima et al., 2001). However, the role of Rim2α in exocytosis has not been clarified. To address this issue, we generated Rim2α$^{-/-}$ mice. In the course of our study, Schoch et al. reported the phenotype of Rim2α$^{-/-}$ mice, which they generated independently, but no changes in blood glucose levels in Rim2α$^{-/-}$ mice were found (Schoch et al., 2006). In the present study, we have analyzed the phenotype of Rim2α$^{-/-}$ mice in detail both *in vivo* and i*n vitro*.

We recently reported that K^+-induced exocytosis comprises mainly granules already docked to the plasma membrane (*old face*), while glucose-induced exocytosis consists almost exclusively of granules that are newly recruited to the plasma membrane (*restless newcomer*) (Shibasaki et al., 2007). In the present study, we show that a mutant Rim2α (E36A/R37S) that does not bind to Rab3A did not rescue docked granules in Rim2α$^{ko/ko}$ β-cells, but was able to rescue glucose-induced insulin

secretion to a degree similar to that rescued by WT Rim2α. This finding indicates that although docking of insulin granules to the plasma membrane requires interaction of Rim2α and Rab3A, it is not essential for glucose-induced insulin secretion. Indeed, despite the defect in docking, K^+-induced insulin secretion is significantly increased in granuphilin$^{-/-}$ mice (Gomi et al., 2005).

It has been thought that the priming and fusion steps occur after the docking step in neuronal cells (Verhage et al., 2008). The priming step is proposed to be initiated by unfolding of the SNARE protein Syntaxin1 from the closed to the open state, which can bind SNAP25 and VAMP2, which are other SNARE proteins, to form the SNARE complex. The mutant Syntaxin1 (L166A/E167A), which is a constitutively open form (Dulubova et al., 1999), can rescue the fusion of synaptic vesicles in *C. elegans* Syntaxin null mutants (Richmond et al., 2001). Although Munc13-1 is thought to be a priming factor in large dense-core and synaptic vesicles, and the interaction of Rim1α and Munc13-1 is thought to regulate priming (Ashery et al., 2000; Betz et al., 2001), the molecular mechanism of the priming step has not been clarified. In Rim1α$^{-/-}$ brain, the expression level of Munc13-1 is decreased (Schoch et al., 2002), and Munc13-1 is not enriched at the active zone of mossy fiber terminals of mouse hippocampus (Andrews-Zwilling et al., 2006). We found that both the expression level and the localization of Munc13-1 are not changed in Rim2α$^{ko/ko}$ β-cells, but that Munc13-1 dissociates from the Rim2α-Munc13-1 complex by glucose stimulation and activates Syntaxin1 to evoke fusion. Rim2α is thus a critical molecule in determining both the docking and priming states in accord with its interacting partner Rab3A or Munc13-1, respectively (Figure S3).

We previously showed that Rim2α is involved in cAMP-induced, PKA-independent insulin secretion through the Epac2 pathway (Ozaki et al., 2000; Kashima et al., 2001). We show here that glucose-induced insulin secretion potentiated by the Epac-specific analog 8-pCPT-2'-*O*-Me-cAMP-AM is not induced in Rim2α$^{ko/ko}$ β-cells expressing mutant Rim2α (PDZ-AAA). This further confirms that Rim2α is required in the Epac2 pathway for potentiation of insulin secretion by cAMP. Because Epac2 also activates Rap1 by cAMP, which may increase the size of the non-docked granule pool and/or facilitate the recruitment of granules to the plasma

membrane (Shibasaki et al., 2007, Seino et al., 2009), both Rim2α and Rap1 act cooperatively in cAMP-induced, Epac2 dependent insulin secretion.

In this study, we also found that Rim2α exerts a suppressive effect on the voltage dependence of inactivation of voltage-dependent Ca^{2+} channel (VDCC) currents, and controls the intracellular Ca^{2+} concentration in pancreatic β-cells (Figure S4), as was found of Rim1α in neurons (Kiyonaka et al., 2007). Rim2α has been shown to interact with VDCCs directly or indirectly (Hibino et al., 2002; Shibasaki et al., 2004). It is generally accepted that neuronal secretion represents vesicle fusion in response to Ca^{2+} microdomains, which requires close proximity of the vesicles to the sites of focal Ca^{2+} entry (Llinas et al., 1992; Barg et al., 2001; Hoppa et al., 2009). These findings together with the role of Rim2α further suggest the importance of the Ca^{2+} microdomain for insulin granule exocytosis in pancreatic β-cells. Rim2α is expressed predominantly in endocrine and neuroendocrine cells (Ozaki et al., 2000). Since we found defects in the secretion of various hormones including GIP, GH, and epinephrine, all of which are stored as dense-core vesicles, Rim2α might well play a similar role in exocytosis of these hormones.

Experimental procedures

Reagents

A full list of reagents is provided in Supplemental Experimental Procedures.

Generation of Rim2α$^{-/-}$ mice

Rim2α$^{-/-}$ mice were generated by replacing the amino acid coding sequences in exon 4 of mouse Rim2 with Neo cassette as described (Figure S1). Detailed description and genotyping strategy are provided in Supplemental Experimental Procedures.

Generation of Rim2α-deficient clonal pancreatic β-cells

Clonal pancreatic β-cells lacking Rim2α (Rim2α$^{ko/ko}$ β-cells) were established by crossbreeding Rim2α$^{-/-}$ mice and *IT6* mice expressing SV40 large T antigen under human insulin promoter that developed highly differentiated β-cell tumors (Miyazaki et at., 1990). Twenty-seven lines of Rim2α$^{ko/ko}$ β-cells were generated from a 10-week-old mouse lacking Rim2α and carrying a large T antigen load (Rim2α$^{-/-}$; *IT6* mouse) as previously described (Shibasaki et al., 2007).

Cell culture

MIN6 cells, Rim2α$^{ko/ko}$ β-cells, and COS-1 cells were grown in Dulbecco's modified Eagle's medium (DMEM) containing 10% heat-inactivated fetal bovine serum and maintained in a humidified incubator with 95% air and 5% CO_2 at 37°C.

RNA extraction and quantitative RT-PCR

Total RNA from mouse pancreatic islets and β-cell lines was isolated using the RNeasy Kit. For reverse transcription, ReverTra Ace-α-Kit was used. Quantitative real-time PCR was carried out by SYBR Premix Ex Taq^{TM} with the primers for mouse Rim2α (forward 5′-GGAAAATCATCCTGGCTGTC and reverse 5′-ATGTCACTGGCAATCTGGTG), mouse Rim2β (forward 5′-ACGAAGTCCATCAGTGTCCA and reverse 5′-GCTCAGACCATTCCAAATCC), and HPRT (forward 5′-TCTTTGCTGACCTGCTGGATT and reverse 5′-GGCTTTGTATTTGGCTTTTCC) using a model 7000 thermal cycler (Applied Biosystems, Foster City, CA). HPRT was used as internal control (Figure S1).

***In vivo* experiments**

Glucose (1.5 g/kg body weight), mixed meal (Twinline: 10 ml/kg body weight), or insulin (0.4 IU/kg body weight) was administered intraperitoneally or orally to overnight (16 h)-fasted male mice at 16-22 weeks of age as described previously (Miki et al., 2005). Blood glucose levels were measured by Antsense III glucose analyzer (Bayer Yakuhin, Osaka, Japan); ELISA system was used for

measurement of serum insulin (Morinaga, Tokyo, Japan), GIP and GH (LINCO Research, St. Charles, MO), and IGF-1 (R&D Systems, Minneapolis, MN). Measurements of epinephrine levels were performed by SRL (Tokyo, Japan).

Immunohistological analysis

The pancreases were removed from Rim2α$^{+/+}$ and Rim2α$^{-/-}$ mice, and were immersion-fixed in 4% paraformaldehyde in 0.1 M phosphate buffer (pH 7.4). Fixed tissues were dehydrated and embedded in paraffin by conventional procedure. Five-micrometer-thick paraffin sections were stained with guinea pig anti-insulin antibody and mouse anti-glucagon antibody, followed by Alexa Fluor 546-conjugated goat anti-guinea pig IgG antibody and Alexa Fluor 488-conjugated goat anti-mouse IgG antibody, respectively. The immunostained tissues were observed by BZ9000 microscope (Keyence, Osaka, Japan).

Immunocytochemical analysis

MIN6 cells and Rim2α$^{ko/ko}$ β-cells were fixed with 3.7% formaldehyde in 0.1 M phosphate buffer (pH 7.4) for 10 min at room temperature and thoroughly rinsed with 0.1 M PBS. After the samples were pretreated with 0.1% Triton X-100 and 10% normal goat serum, they were incubated with guinea pig anti-insulin antibody and rabbit anti-Rim2 antibody, followed by Alexa Fluor 546-conjugated goat anti-guinea pig IgG antibody and Alexa Fluor 488-conjugated goat anti-rabbit IgG antibody, respectively. The immunostained cells were observed by confocal laser scanning microscopy (FV1000; Olympus, Tokyo, Japan).

Insulin secretion experiments

Pancreatic islets were isolated from Rim2α$^{+/+}$ and Rim2α$^{-/-}$ mice by collagenase digestion and cultured for 2 days as described previously (Kashima et al., 2001). Thirty min after preincubation of isolated islets with HEPES-KRB buffer containing 2.8 mM glucose, five size-matched islets were

collected in each well of a 96-well plate and incubated for 30 min in 100 μl of the same buffer containing various stimuli. Insulin released in the incubation buffer and cellular insulin content were measured by ELISA (Medical Biological Laboratories, Nagoya, Japan). The amount of insulin secretion was normalized by cellular insulin content. Insulin secretion experiments in MIN6 cells and Rim2α$^{ko/ko}$ β-cells were performed as described above.

TIRFM analysis

Primary cultured β-cells isolated from mouse pancreatic islets were infected with adenovirus carrying insulin-Venus and subjected to analysis by TIRFM as previously described (Shibasaki et al., 2007). The number of granules docked to the plasma membrane was measured by G-Count software (G-Angstrom K.K, Miyagi, Japan).

Subcellular fractionation

Discontinuous sucrose gradient fractionation of MIN6 cells and Rim2α$^{ko/ko}$ β-cells were carried out as previously described (Sugawara et al., 2009).

Co-immunoprecipitation experiments

Two days before co-immunoprecipitation experiments, COS-1 cells were transiently transfected with plasmids encoding FLAG-tagged Rab3A (Q81L) using Effectene Transfection Reagent (Qiagen) according to the manufacturer's instruction. Co-immunoprecipitation experiments were performed using Pierce Mammalian c-Myc Tag IP/Co-IP Kit (Thermo Fisher Scientific, Waltham, MA) according to the manufacture's instruction. Briefly, Rim2α$^{ko/ko}$ β-cells were infected with Ad-β-galactosidase (β-gal) or Ad-Rim2α. After 2-day culture, the infected cells were preincubated in HEPES-KRB buffer containing 2.8 mM glucose. Thirty min after preincubation, the cells were stimulated with HEPES-KRB buffer containing 2.8 mM glucose or 25 mM glucose for 30 min. The cells were then lysed in buffer containing 10 mM HEPES (pH 7.4), 150 mM NaCl, 0.5% CHAPS, 5

mM $MgCl_2$, and protease inhibitor cocktail, and collected in microcentrifuge tubes. The cellular lysates were incubated with 10 μl anti-c-Myc antibody conjugated with agarose in the absence or presence of cellular lysate of COS-1 transfected with FLAG-tagged Rab3A (Q81L). After incubation at 4°C for overnight, the agarose was washed five times with buffer containing 25 mM Tris-HCl, 150 mM NaCl, and 0.05% Tween 20 (pH7.2), and the bound proteins were subjected to SDS-PAGE followed by immunoblot analysis with anti-Rim2, anti-Munc13, and anti-Rab3 antibodies.

Construction of adenovirus vectors

Rat Rab3A was subcloned into pFLAG-CMV-2 vector (Sigma). Site-directed mutagenesis of the N-terminal Zn^{2+}-finger domain (E36A/R37S and K136E/K138E mutants) and PDZ domain (PDZ-AAA mutant) in mouse Rim2α and L166A/E167A mutant in mouse Syntaxin1 was performed by the PCR-based method. Recombinant adenovirus carrying c-Myc tagged WT Rim2α (Ad-Rim2α) or c-Myc tagged mutants of Rim2α (Ad-Rim2α mutants) were generated according to the manufacturer's instruction (Stratagene, La Jolla, CA).

Perifusion experiments

Perifusion experiments on insulin secretion of $Rim2\alpha^{ko/ko}$ β-cells were performed as described previously (Sugawara et al., 2009). Briefly, the cells were seeded at a density of 5×10^5 cells on coverslips. The following day, the cells were infected with Ad-β-gal or Ad-Rim2α mutants or Ad-Syntaxin1 at an MOI of 1 and maintained for 48 h. The cells were then incubated in HEPES-KRB containing 2.8 mM glucose for 50 min and mounted in a perifusion chamber. The cells were perifused in KRBH containing 2.8 mM glucose for 5 min, and the perfusate was then switched to HEPES-KRB containing 25 mM glucose or 60 mM K^+. Eluted fractions were collected at 1-min intervals, and released insulin in each fraction was measured by insulin assay kit (CIS bio international, Gif sur Yvette, France). The amount of secreted insulin was normalized by cellular insulin contents.

Statistical Analysis

The data are expressed as means ± SEM. Comparisons were made using Student's unpaired *t*-test, Dunnet's method, or Tukey-Kramer's method as indicated in the legends. A probability level of $p < 0.05$ was considered statistically significant.

Acknowledgments

This work was supported by a CREST grant from the Japan Science and Technology Agency and Grant-in-Aid for Scientific Research and by a grant for the Global Centers of Excellence Program "Global Center of Excellence for Education and Research on Signal Transduction Medicine in the Coming Generation" and "Global Center for Education and Research in Integrative Membrane Biology" from the Ministry of Education, Culture, Sports, Science and Technology.

References

Andrews-Zwilling, Y. S., Kawabe, H., Reim, K., Varoqueaux, F., and Brose, N. (2006). Binding to Rab3A-interacting molecule RIM regulates the presynaptic recruitment of Munc13-1 and ubMunc13-2. J. Biol. Chem. *281*, 19720-19731.

Ashery, U., Varoqueaux, F., Voets, T., Betz, A., Thakur, P., Koch, H., Neher, E., Brose, N., and Rettig, J. (2000). Munc13-1 acts as a priming factor for large dense-core vesicles in bovine chromaffin cells. EMBO J. *19*, 3586-3596.

Barg, S., Ma, X., Eliasson, L., Galvanovskis, J., Göpel, S. O., Obermüller, S., Platzer, J., Renström, E., Trus, M., Atlas, D., Striessnig, J., Rorsman, P. (2001). Fast exocytosis with few Ca^{2+} channels in

insulin-secreting mouse pancreatic B cells. Biophys. J. *81*, 3308-3323.

Betz, A., Ashery, U., Rickmann, M., Augustin, I., Neher, E., Sudhof, T. C., Rettig, J., and Brose, N. (1998). Munc13-1 is a presynaptic phorbol ester receptor that enhances neurotransmitter release. Neuron *21*, 123-136.

Betz, A., Thakur, P., Junge, H. J., Ashery, U., Rhee, J. S., Scheuss, V., Rosenmund, C., Rettig, J., and Brose, N. (2001). Functional interaction of the active zone proteins Munc13-1 and RIM1 in synaptic vesicle priming. Neuron *30*, 183-196.

Brondyk, W. H., McKiernan, C. J., Burstein, E. S., and Macara, I. G. (1993). Mutants of Rab3A analogous to oncogenic Ras mutants. Sensitivity to Rab3A-GTPase activating protein and Rab3A-guanine nucleotide releasing factor. J. Biol. Chem. *268*, 9410-9415.

Brunner, Y., Coute, Y., Iezzi, M., Foti, M., Fukuda, M., Hochstrasser, D. F., Wollheim, C. B., and Sanchez, J. C. (2007). Proteomics analysis of insulin secretory granules. Mol. Cell. Proteomics *6*, 1007-1017.

Burgoyne, R. D., and Morgan, A. (2003). Secretory granule exocytosis. Physiol. Rev. *83*, 581-632.

Castillo, P. E., Schoch, S., Schmitz, F., Sudhof, T. C., and Malenka, R. C. (2002). RIM1α is required for presynaptic long-term potentiation. Nature *415*, 327-330.

Drucker, D. J. (2006). The biology of incretin hormones. Cell Metab. *3*, 153-165.

Dulubova, I., Lou, X., Lu, J., Huryeva, I., Alam, A., Schneggenburger, R., Sudhof, T. C., and Rizo, J.

(2005). A Munc13/RIM/Rab3 tripartite complex: from priming to plasticity? EMBO J. *24*, 2839-2850.

Dulubova, I., Sugita, S., Hill, S., Hosaka, M., Fernandez, I., Sudhof, T. C., and Rizo, J. (1999). A conformational switch in syntaxin during exocytosis: role of munc18. EMBO J. *18*, 4372-4382.

Fujimoto, K., Shibasaki, T., Yokoi, N., Kashima, Y., Matsumoto, M., Sasaki, T., Tajima, N., Iwanaga, T., and Seino, S. (2002). Piccolo, a Ca^{2+} sensor in pancreatic β-cells. Involvement of cAMP-GEFII·Rim2·Piccolo complex in cAMP-dependent exocytosis. J. Biol. Chem. *277*, 50497-50502.

Fukuda, M. (2003). Distinct Rab binding specificity of Rim1, Rim2, Rabphilin, and Noc2. Identification of a critical determinant of Rab3A/Rab27A recognition by Rim2. J. Biol. Chem. *278*, 15373-15380.

Fukuda, M. (2004). Alternative splicing in the first α-helical region of the Rab-binding domain of Rim regulates Rab3A binding activity: is Rim a Rab3 effector protein during evolution? Genes Cells *9*, 831-842.

Fukui, K., Yang, Q., Cao, Y., Takahashi, N., Hatakeyama, H., Wang, H., Wada, J., Zhang, Y., Marselli, L., Nammo, T., *et al.* (2005). The HNF-1 target collectrin controls insulin exocytosis by SNARE complex formation. Cell Metab. *2*, 373-384.

Gomi, H., Mizutani, S., Kasai, K., Itohara, S., and Izumi, T. (2005). Granuphilin molecularly docks insulin granules to the fusion machinery. J. Cell Biol. *171*, 99-109.

Hibino, H., Pironkova, R., Onwumere, O., Vologodskaia, M., Hudspeth, A. J., and Lesage, F. (2002). RIM binding proteins (RBPs) couple Rab3-interacting molecules (RIMs) to voltage-gated Ca^{2+} channels. Neuron *34*, 411-423.

Hoppa, M. B., Collins, S., Ramracheya, R., Hodson, L., Amisten, S., Zhang, Q., Johnson, P., Ashcroft, F. M., Rorsman, P. (2009). Chronic palmitate exposure inhibits insulin secretion by dissociation of Ca^{2+} channels from secretory granules. Cell Metab. *10*, 455-465.

Inoue, E., Deguchi-Tawarada, M., Takao-Rikitsu, E., Inoue, M., Kitajima, I., Ohtsuka, T., and Takai, Y. (2006). ELKS, a protein structurally related to the active zone protein CAST, is involved in Ca^{2+}-dependent exocytosis from PC12 cells. Genes Cells *11*, 659-672.

Kang, L., He, Z., Xu, P., Fan, J., Betz, A., Brose, N., and Xu, T. (2006). Munc13-1 is required for the sustained release of insulin from pancreatic β cells. Cell Metab. *3*, 463-468.

Kasai, K., Ohara-Imaizumi, M., Takahashi, N., Mizutani, S., Zhao, S., Kikuta, T., Kasai, H., Nagamatsu, S., Gomi, H., and Izumi, T. (2005). Rab27a mediates the tight docking of insulin granules onto the plasma membrane during glucose stimulation. J. Clin. Invest. *115*, 388-396.

Kashima, Y., Miki, T., Shibasaki, T., Ozaki, N., Miyazaki, M., Yano, H., and Seino, S. (2001). Critical role of cAMP-GEFII·Rim2 complex in incretin-potentiated insulin secretion. J. Biol. Chem. *276*, 46046-46053.

Kiyonaka, S., Wakamori, M., Miki, T., Uriu, Y., Nonaka, M., Bito, H., Beedle, A. M., Mori, E., Hara, Y., De Waard, M., *et al.* (2007). RIM1 confers sustained activity and neurotransmitter vesicle anchoring to presynaptic Ca^{2+} channels. Nat. Neurosci. *10*, 691-701.

Koushika, S. P., Richmond, J. E., Hadwiger, G., Weimer, R. M., Jorgensen, E. M., and Nonet, M. L. (2001). A post-docking role for active zone protein Rim. Nat. Neurosci. *4*, 997-1005.

Llinas, R., Sugimori, M., and Silver, R. B. (1992). Microdomains of high calcium concentration in a presynaptic terminal. Science *256*, 677-679.

Lonart, G., Schoch, S., Kaeser, P. S., Larkin, C. J., Sudhof, T. C., and Linden, D. J. (2003). Phosphorylation of RIM1α by PKA triggers presynaptic long-term potentiation at cerebellar parallel fiber synapses. Cell *115*, 49-60.

Madison, J. M., Nurrish, S., and Kaplan, J. M. (2005). UNC-13 interaction with syntaxin is required for synaptic transmission. Curr. Biol. *15*, 2236-2242.

Matsumoto, M., Miki, T., Shibasaki, T., Kawaguchi, M., Shinozaki, H., Nio, J., Saraya, A., Koseki, H., Miyazaki, M., Iwanaga, T., and Seino, S. (2004). Noc2 is essential in normal regulation of exocytosis in endocrine and exocrine cells. Proc. Natl. Acad. Sci. USA *101*, 8313-8318.

Menasche, G., Pastural, E., Feldmann, J., Certain, S., Ersoy, F., Dupuis, S., Wulffraat, N., Bianchi, D., Fischer, A., Le Deist, F., and de Saint Basile, G. (2000). Mutations in RAB27A cause Griscelli syndrome associated with haemophagocytic syndrome. Nat. Genet. *25*, 173-176.

Miki, T., Minami, K., Shinozaki, H., Matsumura, K., Saraya, A., Ikeda, H., Yamada, Y., Holst, J. J., and Seino, S. (2005). Distinct effects of glucose-dependent insulinotropic polypeptide and glucagon-like peptide-1 on insulin secretion and gut motility. Diabetes *54*, 1056-1063.

Miyazaki, J., Araki, K., Yamato, E., Ikegami, H., Asano, T., Shibasaki, Y., Oka, Y., and Yamamura, K. (1990). Establishment of a pancreatic β cell line that retains glucose-inducible insulin secretion: special reference to expression of glucose transporter isoforms. Endocrinology *127*, 126-132.

Nicolson, T. J., Bellomo, E. A., Wijesekara, N., Loder, M. K., Baldwin, J. M., Gyulkhandanyan, A. V., Koshkin, V., Tarasov, A. I., Carzaniga, R., Kronenberger, K.*, et al.* (2009). Insulin storage and glucose homeostasis in mice null for the granule zinc transporter ZnT8 and studies of the type 2 diabetes-associated variants. Diabetes *58*, 2070-2083.

Ohara-Imaizumi, M., Ohtsuka, T., Matsushima, S., Akimoto, Y., Nishiwaki, C., Nakamichi, Y., Kikuta, T., Nagai, S., Kawakami, H., Watanabe, T., and Nagamatsu, S. (2005). ELKS, a protein structurally related to the active zone-associated protein CAST, is expressed in pancreatic β cells and functions in insulin exocytosis: interaction of ELKS with exocytotic machinery analyzed by total internal reflection fluorescence microscopy. Mol. Biol. Cell *16*, 3289-3300.

Ozaki, N., Shibasaki, T., Kashima, Y., Miki, T., Takahashi, K., Ueno, H., Sunaga, Y., Yano, H., Matsuura, Y., Iwanaga, T.*, et al.* (2000). cAMP-GEFII is a direct target of cAMP in regulated exocytosis. Nat. Cell Biol. *2*, 805-811.

Richmond, J. E., Weimer, R. M., and Jorgensen, E. M. (2001). An open form of syntaxin bypasses the requirement for UNC-13 in vesicle priming. Nature *412*, 338-341.

Schoch, S., Castillo, P. E., Jo, T., Mukherjee, K., Geppert, M., Wang, Y., Schmitz, F., Malenka, R. C., and Sudhof, T. C. (2002). RIM1α forms a protein scaffold for regulating neurotransmitter release at the active zone. Nature *415*, 321-326.

Schoch, S., Mittelstaedt, T., Kaeser, P. S., Padgett, D., Feldmann, N., Chevaleyre, V., Castillo, P. E., Hammer, R. E., Han, W., Schmitz, F.*, et al.* (2006). Redundant functions of RIM1α and RIM2α in Ca^{2+}-triggered neurotransmitter release. EMBO J. *25*, 5852-5863.

Seino, S., and Shibasaki, T. (2005). PKA-dependent and PKA-independent pathways for cAMP-regulated exocytosis. Physiol. Rev. *85*, 1303-1342.

Seino, S., Takahashi, H., Fujimoto, W., and Shibasaki, T. (2009). Roles of cAMP signalling in insulin granule exocytosis. Diabetes Obes. Metab. *11 Suppl 4*, 180-188.

Shibasaki, T., Sunaga, Y., Fujimoto, K., Kashima, Y., and Seino, S. (2004). Interaction of ATP sensor, cAMP sensor, Ca^{2+} sensor, and voltage-dependent Ca^{2+} channel in insulin granule exocytosis. J. Biol. Chem. *279*, 7956-7961.

Shibasaki, T., Takahashi, H., Miki, T., Sunaga, Y., Matsumura, K., Yamanaka, M., Zhang, C., Tamamoto, A., Satoh, T., Miyazaki, J., and Seino, S. (2007). Essential role of Epac2/Rap1 signaling in regulation of insulin granule dynamics by cAMP. Proc. Natl. Acad. Sci. USA *104*, 19333-19338.

Sudhof, T. C. (2004). The synaptic vesicle cycle. Annu. Rev. Neurosci. *27*, 509-547.

Sugawara, K., Shibasaki, T., Mizoguchi, A., Saito, T., and Seino, S. (2009). Rab11 and its effector Rip11 participate in regulation of insulin granule exocytosis. Genes Cells *14*, 445-456.

Verhage, M., and Sorensen, J. B. (2008). Vesicle docking in regulated exocytosis. Traffic *9*, 1414-1424.

Vliem, M. J., Ponsioen, B., Schwede, F., Pannekoek, W. J., Riedl, J., Kooistra, M. R., Jalink, K., Genieser, H. G., Bos, J. L., and Rehmann, H. (2008). 8-pCPT-2'-*O*-Me-cAMP-AM: an improved Epac-selective cAMP analogue. Chembiochem *9*, 2052-2054.

Wang, Y., Okamoto, M., Schmitz, F., Hofmann, K., and Sudhof, T. C. (1997). Rim is a putative Rab3 effector in regulating synaptic-vesicle fusion. Nature *388*, 593-598.

Wang, Y., and Sudhof, T. C. (2003). Genomic definition of RIM proteins: evolutionary amplification of a family of synaptic regulatory proteins. Genomics *81*, 126-137.

Figure Legends

Figure 1. Impaired insulin and GIP secretion in Rim2α$^{-/-}$ mice

(A) Changes in blood glucose levels (left) and serum insulin levels (right) after intraperitoneal glucose load in Rim2α$^{+/+}$ mice (white) and Rim2α$^{-/-}$ mice (black).

(B) Changes in blood glucose levels (left) and serum insulin levels (right) after oral glucose load in Rim2α$^{+/+}$ mice (white) and Rim2α$^{-/-}$ mice (black).

(C) Changes in blood glucose levels (left) and serum insulin levels (right) after mixed meal load in Rim2α$^{+/+}$ mice (white) and Rim2α$^{-/-}$ mice (black).

(D) GIP secretion after mixed meal load in Rim2α$^{+/+}$ mice (white) and Rim2α$^{-/-}$ mice (black).

Data were obtained from 3 independent experiments (n = 5-19) and expressed as means ± SEM. *p < 0.01 (Student's unpaired *t*-test).

See also Figure S1.

Figure 2. Impaired insulin secretion in pancreatic islets of Rim2α$^{-/-}$ mice

(A) Insulin contents in pancreatic islets of Rim2α$^{+/+}$ mice (white) and Rim2α$^{-/-}$ mice (black).

(B) Insulin secretion in response to glucose and 60 mM K^+ in pancreatic islets of Rim2$\alpha^{+/+}$ mice (white) and Rim2$\alpha^{-/-}$ mice (black).

(C) Effects of cAMP-increasing agents on insulin secretion in pancreatic islets of Rim2$\alpha^{+/+}$ mice (white) and Rim2$\alpha^{-/-}$ mice (black).

Data were obtained from 2-3 independent experiments (n = 5-9) and expressed as means ± SEM. *p < 0.01 (Student's unpaired *t*-test).

Figure 3. Rim2α-mediated insulin granule exocytosis

(A) Comparison of the number of insulin granules docked to the plasma membrane in pancreatic β-cells of Rim2$\alpha^{+/+}$ and Rim2$\alpha^{-/-}$ mice. Primary cultured pancreatic β-cells were preincubated with HEPES-KRB buffer containing 2.8 mM glucose at 37°C for 30 min, fixed, immunostained with anti-insulin antibody and observed by TIRFM. The surrounding lines represent the outline of a cell attached to the cover glass. The number of docked granules was measured in a cell surface area of 200 μm^2. Scale bar, 10 μm. Data were obtained from 3 independent experiments (n = 8) and expressed as means ± SEM. *p < 0.01 (Student's unpaired *t*-test).

(B) Histogram of fusion events at 30-sec intervals in pancreatic β-cells of Rim2$\alpha^{+/+}$ (left) and Rim2$\alpha^{-/-}$ (right) mice stimulated with 60 mM K^+ in a cell surface area of 200 μm^2. Primary cultured pancreatic β-cells were preincubated with HEPES-KRB buffer containing 2.8 mM glucose at 37°C for 30 min. Thirty seconds after acquisition of the image, the primary cultured cells were stimulated with 60 mM K^+. 2.8 indicates 2.8 mM glucose. *Old face* (Blue): granules that are predocked to the plasma membrane and fused to the membrane by stimulation. *Restless newcomer* (Red): granules that are newly recruited and immediately fused to the plasma membrane by stimulation. *Resting newcomer* (Green): granules that are newly recruited, docked, and fused to the plasma membrane by stimulation. Data were obtained from 5-6 independent experiments (n = 6-7) and expressed as means ± SEM.

(C) Histogram of fusion events in pancreatic β-cells of Rim2$\alpha^{+/+}$ (left) and Rim2$\alpha^{-/-}$ (right) mice

stimulated with 25 mM glucose in a cell surface area of 200 μm^2. Fusion events were analyzed as shown in (B). Data were obtained from 5-6 independent experiments (n = 6-7) and expressed as means ± SEM.

Figure 4. Generation and characterization of Rim2α$^{ko/ko}$ β-cells

(A) Immunocytochemical analysis of MIN6 cells and Rim2α$^{ko/ko}$ β-cells. Green, Rim2; Red, Insulin. Scale bar, 5 μm.

(B) Comparison of expression levels of exocytosis-related proteins among MIN6 cells, Rim2α$^{ko/ko}$ β-cells, and Rim2α$^{ko/ko}$ β-cells expressing WT Rim2α.

(C) Subcellular localization of exocytosis-related proteins in Rim2α$^{ko/ko}$ β-cells. Rim2α$^{ko/ko}$ β-cells were homogenized, and organelles in the supernatants were separated on discontinuous sucrose gradients. Fractions were subjected to immunoblot analysis with anti-Na^+-K^+-ATPase α-1 (plasma membrane marker), Chromogranin-A (large dense-core granule marker), Rim2, Rab3A, Munc13-1, and Syntaxin1.

(D) Insulin secretion from Rim2α$^{ko/ko}$ β-cells. Data were obtained from 3 independent experiments (n = 7-11) and expressed as means ± SEM. *$p < 0.01$ *vs*. corresponding values in Ad-β-gal (Student's unpaired *t*-test).

(E) The number of insulin granules docked to the plasma membrane in Rim2α$^{ko/ko}$ β-cells. Data were obtained from 3 independent experiments (n = 11-16) and expressed as means ± SEM. *$p < 0.01$ *vs*. Ad-β-gal (Student's unpaired *t*-test).

(F) Effect of glucose on the interaction of Rim2α and Rab3A or Munc13-1. After Rim2α$^{ko/ko}$ β-cells expressing c-Myc-tagged WT Rim2α were stimulated with 25 mM glucose for 30 min, their lysates were incubated with lysates of COS-1 cells expressing FLAG-tagged Rab3A (Q81L). Their mixture was subjected to immunoprecipitation with anti-c-Myc antibody-conjugated agarose and then to immunoblot analysis with anti-Rim2, Rab3A, and Munc13-1 antibodies.

See also Figure S2.

Figure 5. Rescue experiments of insulin secretion and the number of docked insulin granules in Rim2α$^{ko/ko}$ β-cells

(A) Effects of mutant Rim2α on insulin secretion and the number of insulin granules docked to the plasma membrane. Upper left panel, glucose- and K^+-induced insulin secretion in Rim2α$^{ko/ko}$ β-cells expressing mutant Rim2α. Upper right panel, the number of insulin granules docked to the plasma membrane in Rim2α$^{ko/ko}$ β-cells expressing mutant Rim2α. In the absence of interaction of Rim2α and Rab3A, insulin granule exocytosis is rather enhanced because the interaction induces docking of insulin granules, which prevents fusion to the plasma membrane (braking) (lower left). In contrast, mutant Rim2α that cannot bind to Munc13-1 but can bind to Rab3A allows the granules to dock. Since priming is not initiated in this state, fusion events do not occur (lower right). *$p < 0.01$ *vs*. corresponding values in Ad-β-gal (Dunnett's method). †$p < 0.01$ *vs*. corresponding values in Ad-WT Rim2α (Tukey-Kramer method).

(B) Effect of PMA stimulation on insulin secretion (left panel) and the number of insulin granules docked to the plasma membrane (middle panel). Right panel, model for insulin granule exocytosis in Rim2α$^{ko/ko}$ β-cells stimulated with PMA. *$p < 0.01$ *vs*. corresponding values in the absence of PMA (Student's unpaired *t*-test).

(C) Effect of Syntaxin1 on insulin secretion (left panel) and the number of insulin granules docked to the plasma membrane (middle panel). Right panel, model for insulin granule exocytosis in Rim2α$^{ko/ko}$ β-cells expressing open Syntaxin1. *$p < 0.01$ *vs*. corresponding values in Ad-β-gal (Dunnett's method).

Data were obtained from 3 independent experiments (n = 7-11) and expressed as means ± SEM. Red, Rim2α; Blue, Rab3A; Green, Munc13-1.

See also Figure S3.

Figure 6. Insulin secretion from perifused Rim2α$^{ko/ko}$ β-cells

(A) Effects of mutant Rim2α on insulin secretion. In the absence of interaction of Rim2α and Rab3A, K^+-induced insulin secretion is enhanced compared to that by WT Rim2α gene transfer. In contrast, mutant Rim2α that cannot bind to Munc13-1 does not restore either glucose- or K^+-induced insulin secretion.

(B) Effect of PMA stimulation on insulin secretion. Insulin secretion is induced by PMA even in the absence of Rim2α.

(C) Effect of Syntaxin1 on insulin secretion induced by glucose (left) and K^+ (right). Open Syntaxin1 rescues both glucose- and K^+-induced insulin secretion.

Data were obtained from 2-3 independent experiments (n = 4-5) and expressed as means ± SEM.

See also Figure S4.

Figure 7. Effect of Rim2α (PDZ-AAA) on Epac2-mediated exocytosis

Rim2α$^{ko/ko}$ β-cells expressing Rim2α (PDZ-AAA) were stimulated with 11.1 mM glucose plus 10 μM 8-pCPT-2'-*O*-Me-cAMP-AM. Data were obtained from 3 independent experiments (n = 8-11) and expressed as means ± SEM. *$p < 0.01$ (Dunnett's method).

Figure 1

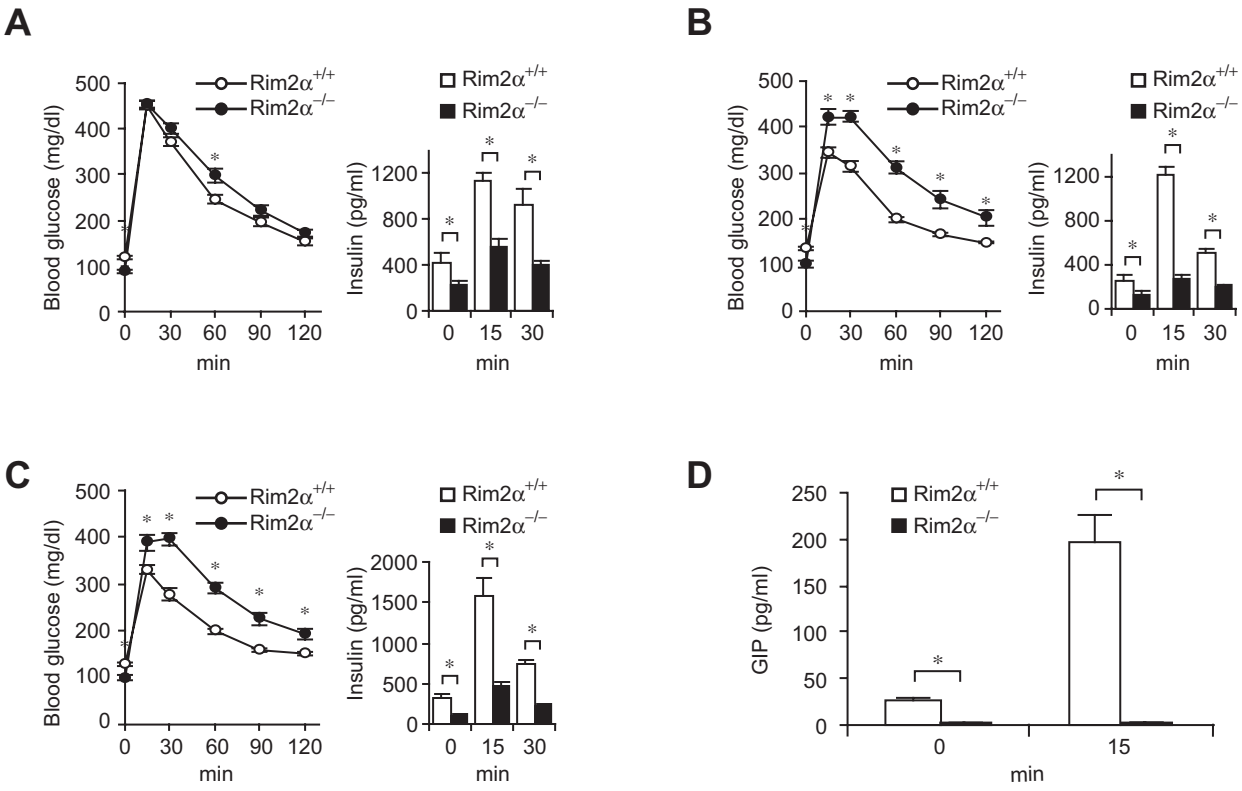
A
B
C
D
Blood glucose (mg/dl)
Insulin (pg/ml)
GIP (pg/ml)
min
Rim2α+/+
Rim2α−/−

Figure 2

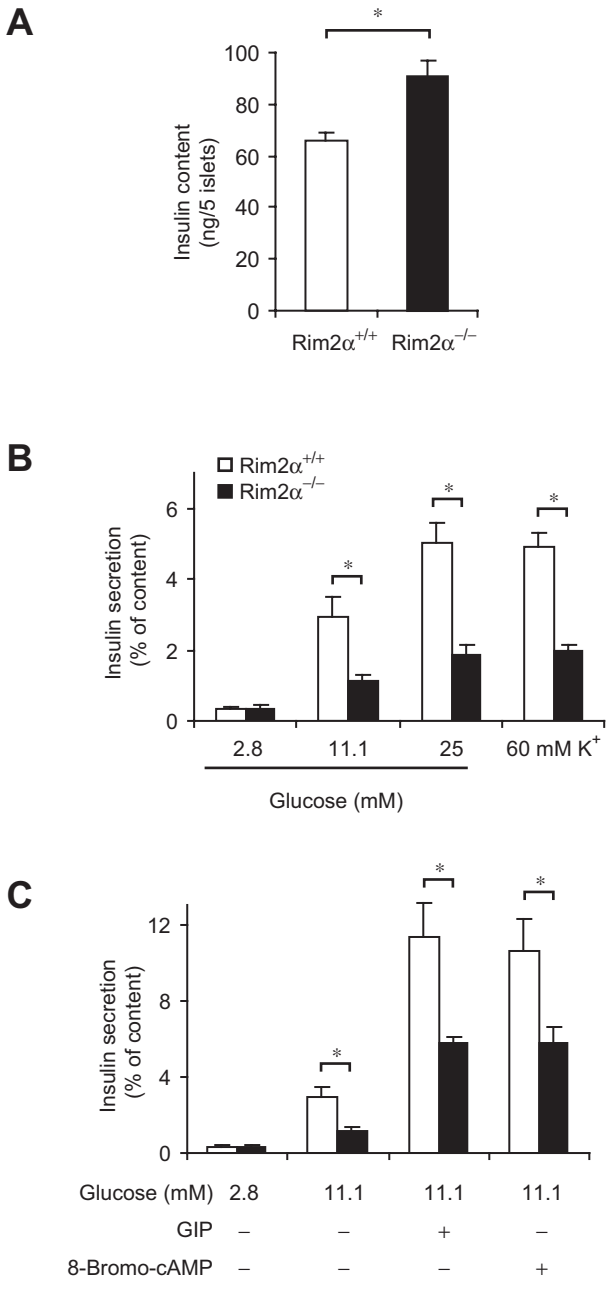
A
*
100
80
60
40
20
0
Insulin content
(ng/5 islets)
Rim2α+/+
Rim2α−/−
B
Rim2α+/+
Rim2α−/−
*
*
*
6
4
2
0
Insulin secretion
(% of content)
2.8
11.1
25
60 mM K+
Glucose (mM)
C
*
*
*
12
8
4
0
Insulin secretion
(% of content)
Glucose (mM) 2.8 11.1 11.1 11.1
GIP – – + –
8-Bromo-cAMP – – – +

Figure 3

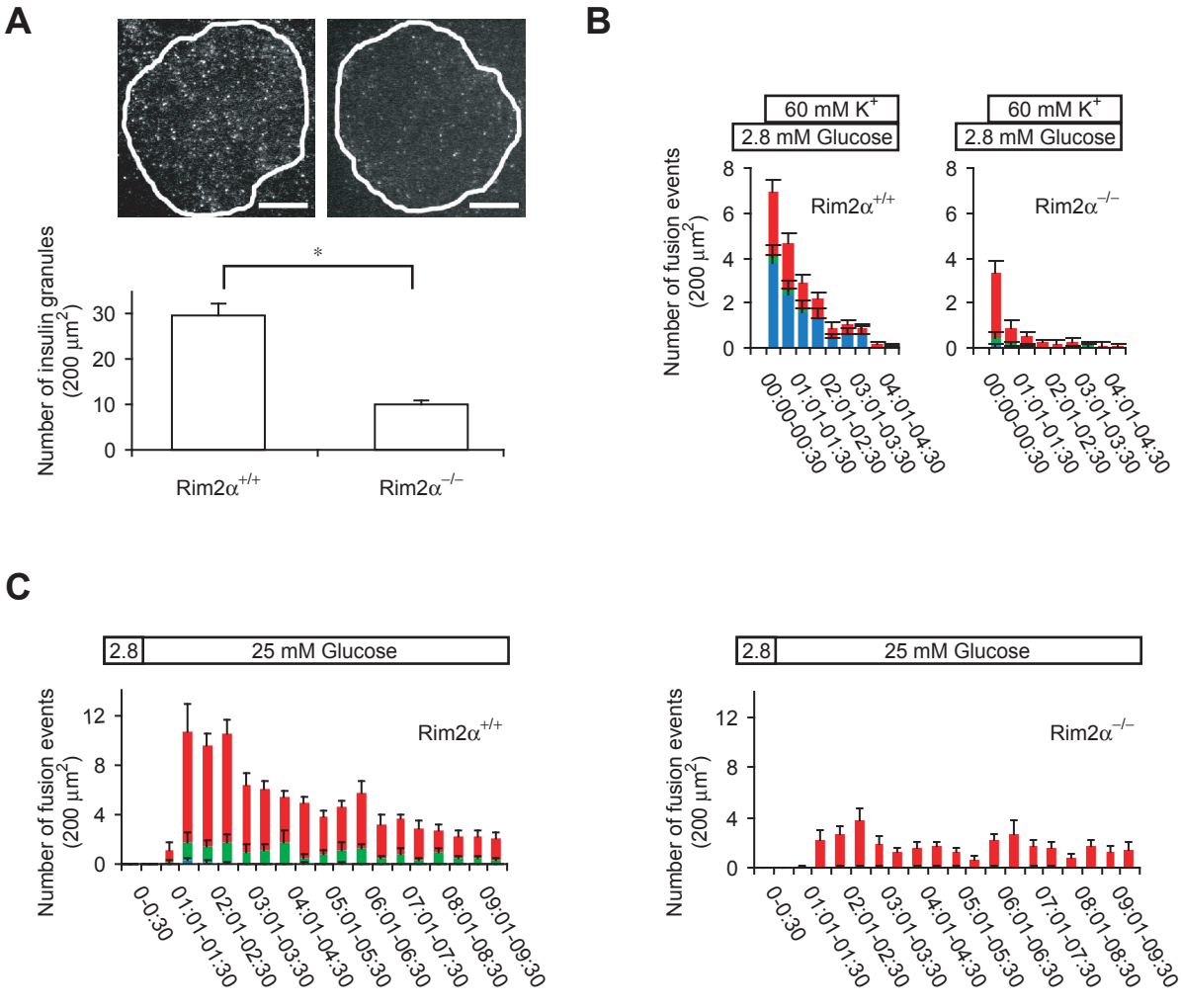
A
Number of insulin granules (200 μm²)
Rim2α+/+
Rim2α−/−
B
60 mM K+
2.8 mM Glucose
Number of fusion events (200 μm²)
Rim2α+/+
Rim2α−/−
00:00-00:30
01:01-01:30
02:01-02:30
03:01-03:30
04:01-04:30
C
2.8
25 mM Glucose
Number of fusion events (200 μm²)
Rim2α+/+
Rim2α−/−
0-0:30
01:01-01:30
02:01-02:30
03:01-03:30
04:01-04:30
05:01-05:30
06:01-06:30
07:01-07:30
08:01-08:30
09:01-09:30

Figure 4

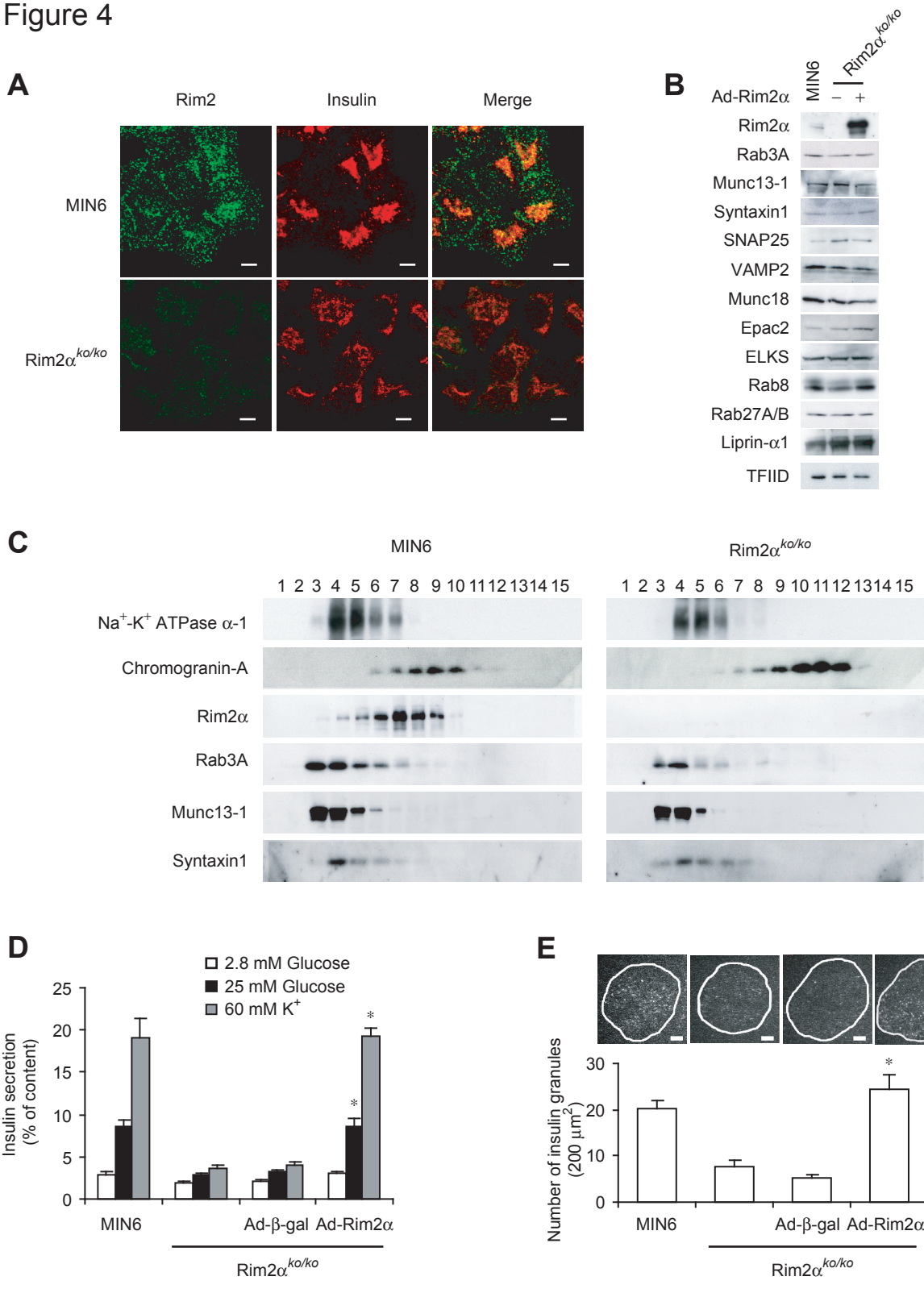
A
Rim2
Insulin
Merge
MIN6
Rim2α ko/ko
B
MIN6
Rim2α ko/ko
Ad-Rim2α
– +
Rim2α
Rab3A
Munc13-1
Syntaxin1
SNAP25
VAMP2
Munc18
Epac2
ELKS
Rab8
Rab27A/B
Liprin-α1
TFIID
C
MIN6
Rim2α ko/ko
1 2 3 4 5 6 7 8 9 10 11 12 13 14 15
Na+-K+ ATPase α-1
Chromogranin-A
Rim2α
Rab3A
Munc13-1
Syntaxin1
D
2.8 mM Glucose
25 mM Glucose
60 mM K+
Insulin secretion (% of content)
0 5 10 15 20 25
MIN6
Ad-β-gal
Ad-Rim2α
Rim2α ko/ko
E
Number of insulin granules (200 μm2)
0 10 20 30
MIN6
Ad-β-gal
Ad-Rim2α
Rim2α ko/ko
F
FLAG-Rab3A (Q81L) – – + +
Ad-Rim2α + + + +
Glucose (mM) 2.8 25 2.8 25
Rim2α
Rab3A
Munc13-1

Figure 5

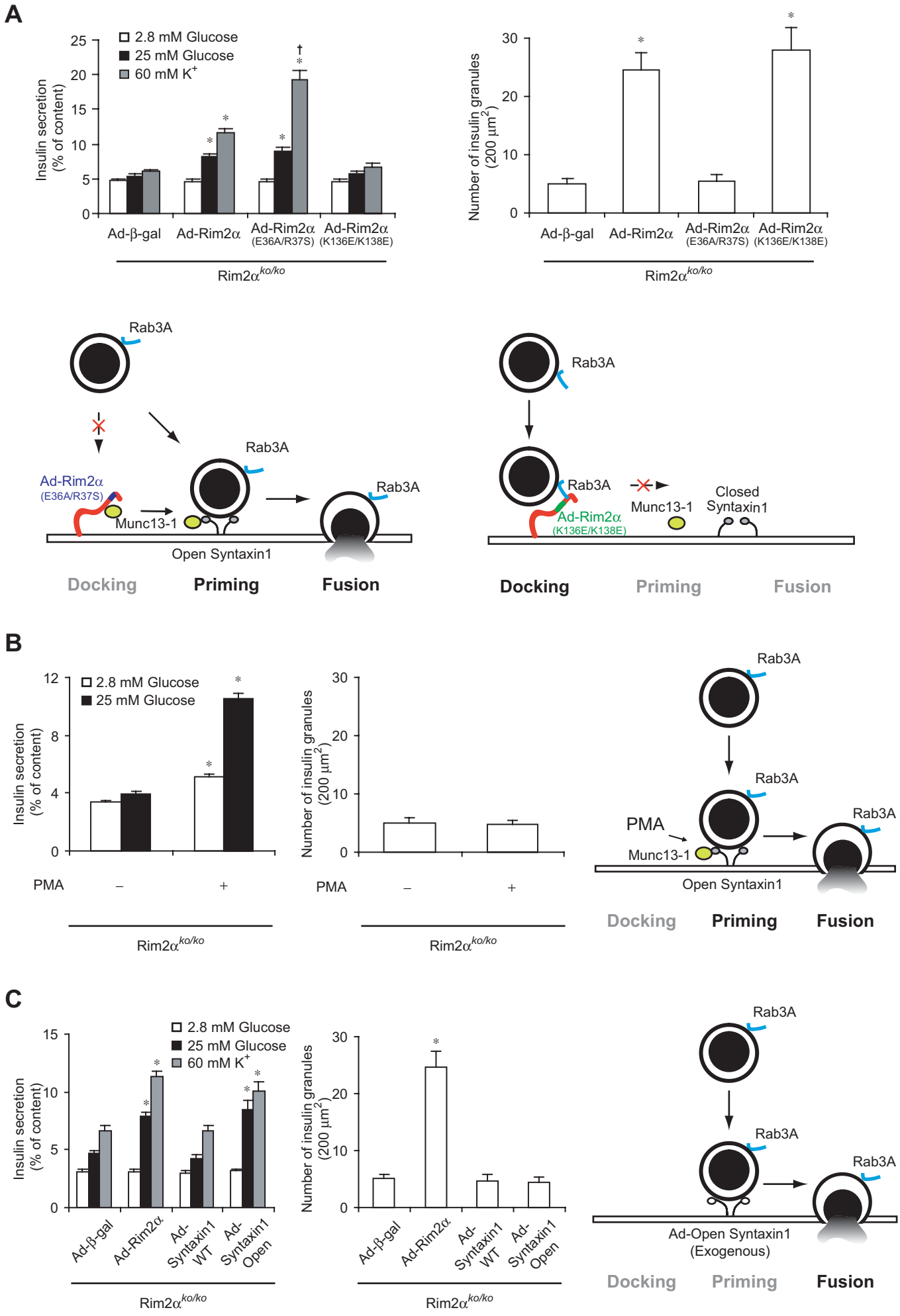
A
2.8 mM Glucose
25 mM Glucose
60 mM K+
Insulin secretion (% of content)
Ad-β-gal
Ad-Rim2α
Ad-Rim2α (E36A/R37S)
Ad-Rim2α (K136E/K138E)
Rim2α ko/ko
Number of insulin granules (200 μm2)
Rab3A
Ad-Rim2α (E36A/R37S)
Munc13-1
Open Syntaxin1
Docking
Priming
Fusion
Ad-Rim2α (K136E/K138E)
Closed Syntaxin1
B
PMA
C
Ad-Syntaxin1 WT
Ad-Syntaxin1 Open
Ad-Open Syntaxin1 (Exogenous)

Figure 6

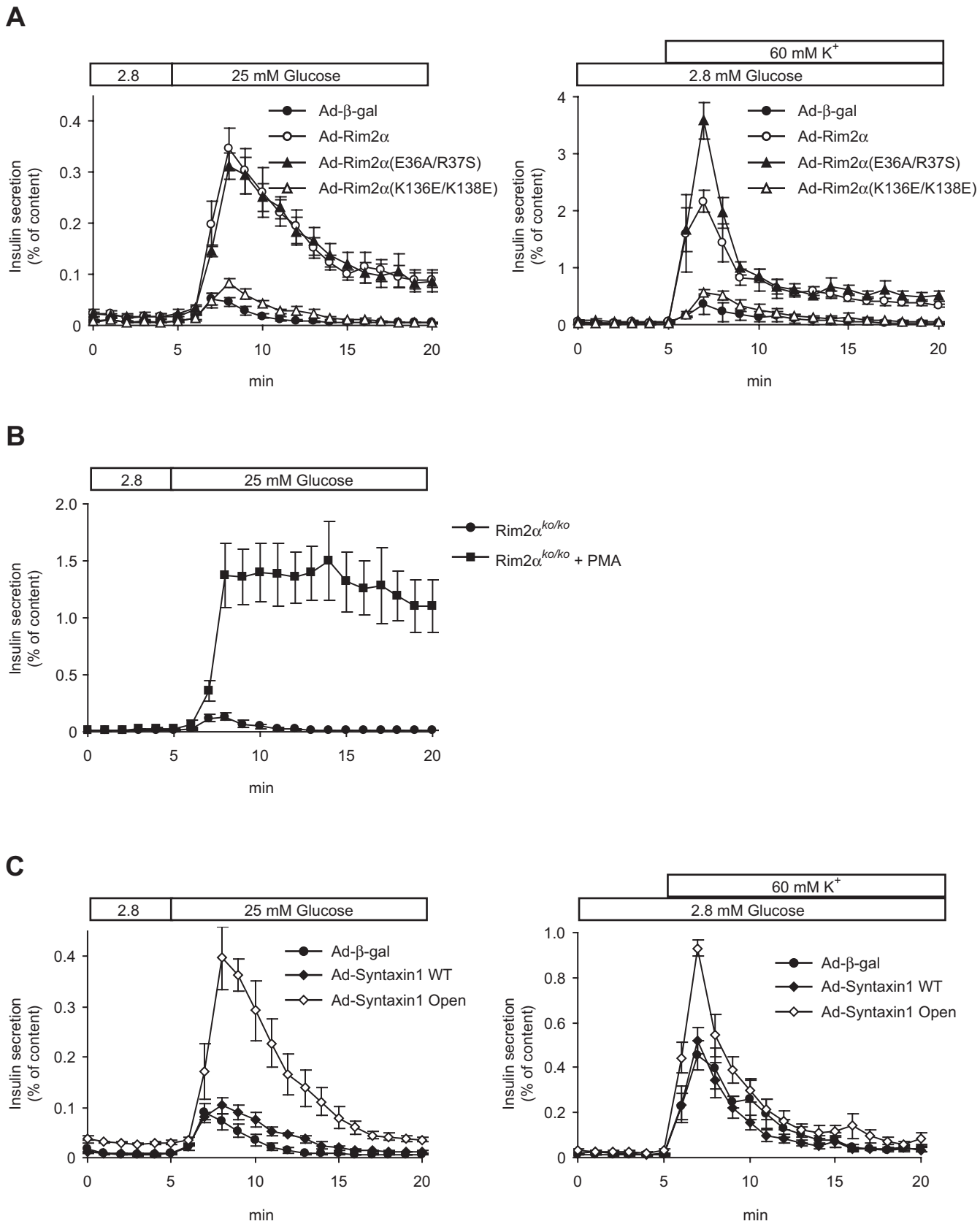
A
2.8
25 mM Glucose
Ad-β-gal
Ad-Rim2α
Ad-Rim2α(E36A/R37S)
Ad-Rim2α(K136E/K138E)
Insulin secretion (% of content)
min
60 mM K+
2.8 mM Glucose
B
Rim2α ko/ko
Rim2α ko/ko + PMA
C
Ad-Syntaxin1 WT
Ad-Syntaxin1 Open

Figure 7

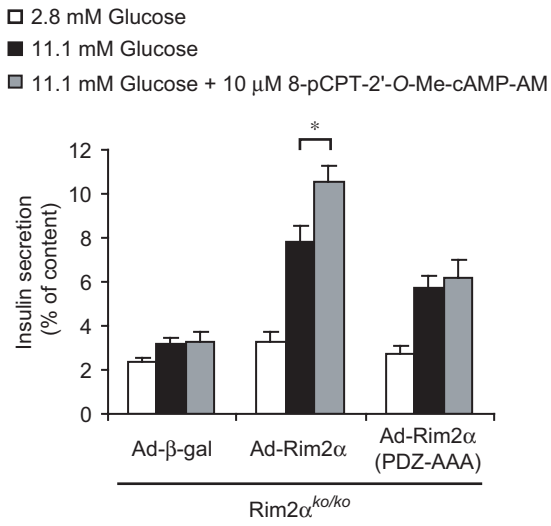
2.8 mM Glucose
11.1 mM Glucose
11.1 mM Glucose + 10 μM 8-pCPT-2'-O-Me-cAMP-AM
Insulin secretion (% of content)
0
2
4
6
8
10
12
*
Ad-β-gal
Ad-Rim2α
Ad-Rim2α (PDZ-AAA)
Rim2α^ko/ko

Supplemental Information

Figure S1

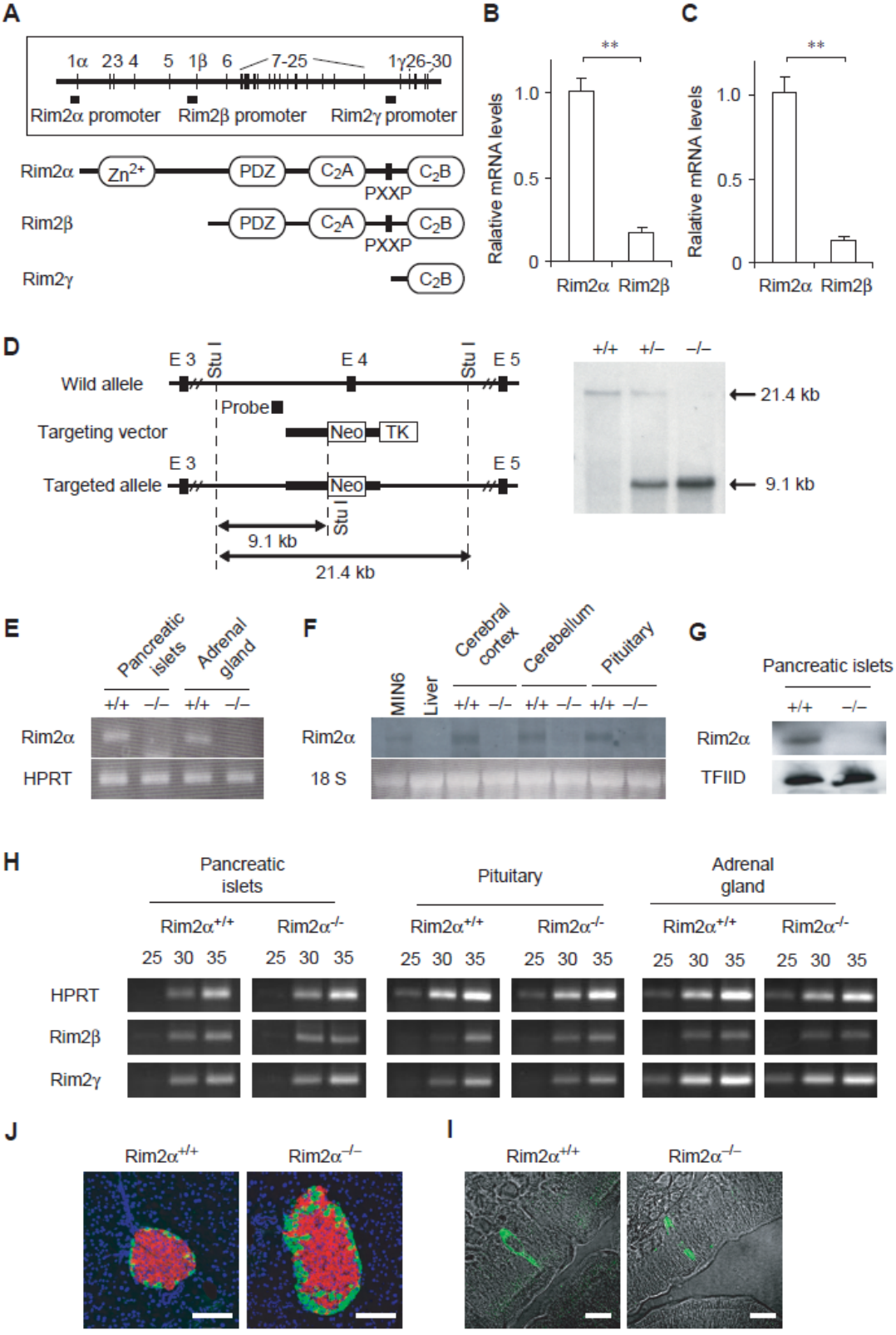

Figure S1 continued

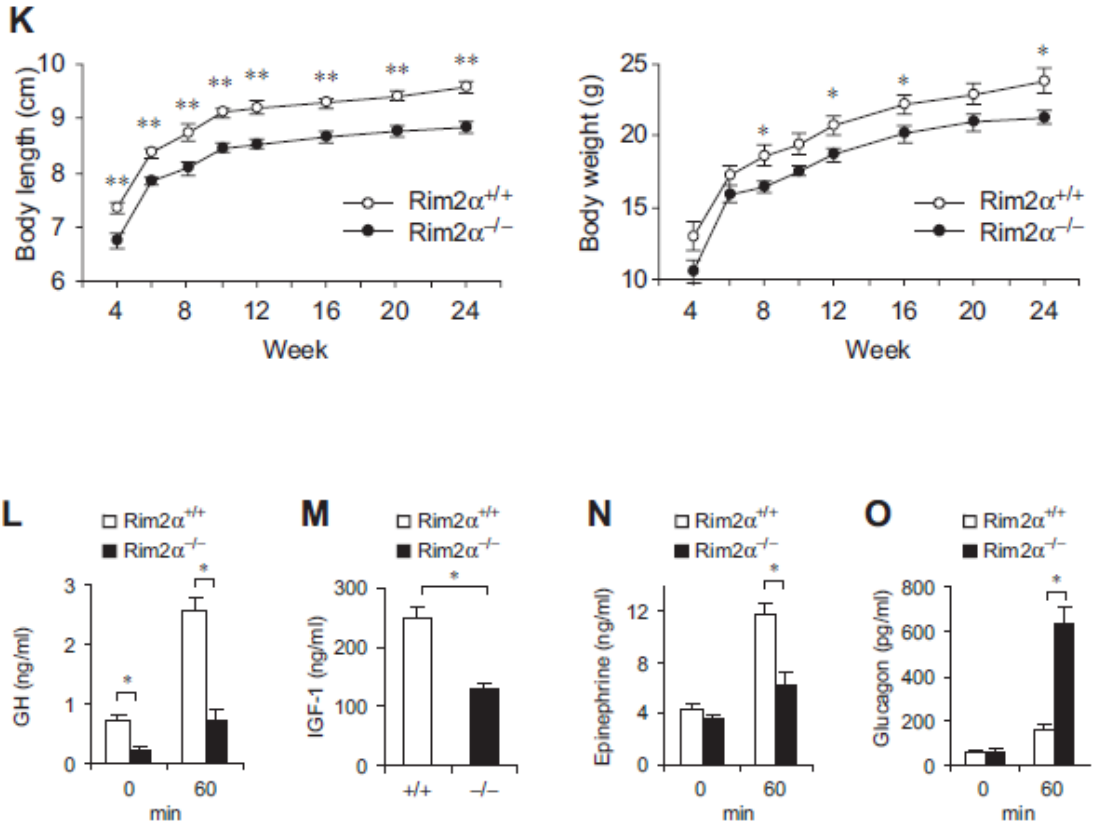

Figure S1. Generation and characterization of Rim2α$^{-/-}$ mice

(A) Structure of the Rim2 gene and domain structure of Rim2 isoforms. Exons are identified by numbers. Zn^{2+}, Zn^{2+}-finger domain; PDZ, PDZ domain; C_2A and C_2B, C_2A and C_2B domain; PXXP, proline-rich region.

(B) Quantitative real-time RT-PCR analysis of Rim2 genes in pancreatic islets. Rim2α mRNA is expressed mainly in pancreatic islets.

(C) Quantitative real-time RT-PCR analysis of Rim2 genes in MIN6 cells. Rim2α mRNA is expressed mainly in MIN6 cells.

(D) Schematic representation of the mouse Rim2α gene, targeting vector, and targeted allele, and Southern blot analysis of F1 offspring. Exons are indicated by arrows. Neo and TK indicate a neomycin-resistant gene and a herpes simplex virus thymidine kinase gene, respectively. Restriction sites are indicated. The probe used for Southern blot analysis is shown. Genomic DNA was digested with Stu I and hybridized with the probe. Lanes: +/+, wild-type; +/-, heterozygote; -/-; homozygote.

(E) RT-PCR analysis of pancreatic islets and adrenal gland of Rim2α$^{+/+}$ mice and Rim2α$^{-/-}$ mice. Rim2α transcript was not detected in these tissues of Rim2α$^{-/-}$ mice. Lanes: +/+, Rim2α$^{+/+}$ mice; -/-, Rim2α$^{-/-}$ mice.

(F) Northern blot analysis. Total RNA (20 μg) from cerebral cortex, cerebellum and pituitary of Rim2α$^{+/+}$ mice and Rim2α$^{-/-}$ mice was used.

(G) Immunoblot analysis of pancreatic islets of Rim2α$^{+/+}$ mice and Rim2α$^{-/-}$ mice. Lanes: +/+, Rim2α$^{+/+}$ mice; -/-, Rim2α$^{-/-}$ mice

(H) Double immunostaining of pancreas of Rim2α$^{+/+}$ mouse and Rim2α$^{-/-}$ mouse for glucagon (green) and insulin (red). Pancreatic islets of Rim2α$^{-/-}$ mice are larger than those of Rim2α$^{+/+}$ mice. Scale bars, 100 μm.

(I) Immunostaining of intestinal K cells of Rim2α$^{+/+}$ mouse and Rim2α$^{-/-}$ mouse for GIP (green). Scale bars, 10 μm.

(J) RT-PCR analysis for Rim2 variants in pancreatic islets, pituitary, and adrenal gland of Rim2α$^{+/+}$ mice and Rim2α$^{-/-}$ mice. Expression levels of Rim2β and Rim2γ in Rim2α$^{-/-}$ mice are similar to those in Rim2α$^{+/+}$ mice.

(K) Body length (Left) and body weight (Right) of Rim2α$^{+/+}$ mice and Rim2α$^{-/-}$ mice. Rim2α$^{-/-}$ mice are smaller than Rim2α$^{+/+}$ mice.

(L) GH secretion in response to insulin administration. GH secretion from Rim2α$^{-/-}$ mice is significantly decreased.

(M) IGF-1 in Rim2α$^{+/+}$ mice and Rim2α$^{-/-}$ mice at steady state. IGF-1 level is decreased in Rim2α$^{-/-}$ mice.

(N) Epinephrine secretion in response to insulin administration. Epinephrine secretion from Rim2α$^{-/-}$ mice is decreased after insulin administration.

(O) Glucagon secretion in response to insulin administration. Glucagon secretion from Rim2α$^{-/-}$ mice is significantly increased after insulin administration.

Data were obtained from 2-3 independent experiments (n = 4-12) and expressed as means ± SEM. *$p < 0.05$, **$p < 0.01$ (Student's unpaired *t*-test).

Figure S2, related to Figure 4

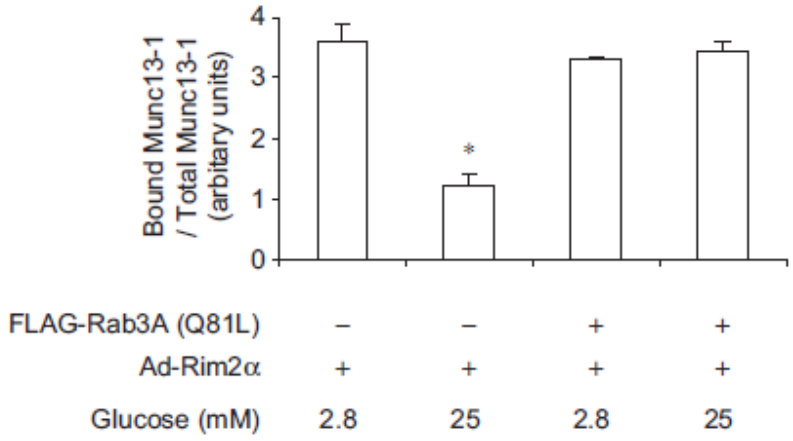

Figure S2. Effect of glucose on the interaction of Rim2α and Munc13-1

After Rim2α$^{ko/ko}$ β-cells expressing c-Myc-tagged WT Rim2α were stimulated with 25 mM glucose for 30 min, their lysates were incubated with lysates of COS-1 cells expressing FLAG-tagged Rab3A (Q81L). The mixture was subjected to immunoprecipitation with anti-c-Myc antibody-conjugated agarose and then to immunoblot analyses with Munc13-1 antibody. Blots shown in Figure 4 were quantified by densitometry. Data were obtained from 3 independent experiments (n = 3) and expressed as means ± SEM. *$p < 0.01$ *vs.* 2.8 mM glucose stimulation without FLAG-Rab3A (Q81L) (Dunnett's method).

Figure S3, related to Figure 5

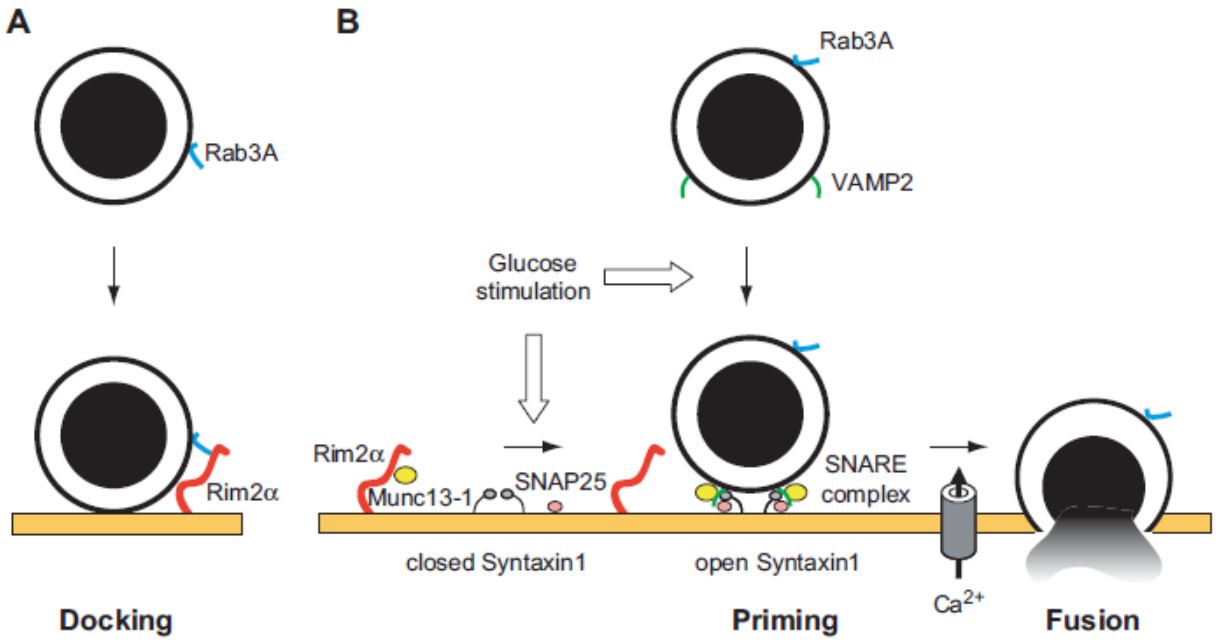

Figure S3. A model for roles of Rim2α in insulin granule exocytosis

(A) Insulin granules are docked to the plasma membrane by interacting Rim2α and Rab3A, a state that prevents fusion (braking). (B) At basal state, Rim2α interacts with Munc13-1. After glucose stimulation, insulin granules (restless newcomer) are recruited to the plasma membrane while Munc13-1 dissociates from the Rim2α/Mnc13-1 complex and activates Syntaxin1 to form a stable SNARE complex with its cognate partners, SNAP25 and VAMP2 (priming). Red, Rim2α; Blue, Rab3A; Yellow, Munc13-1; Pink, SNAP25; Green, VAMP2; Gray, Syntaxin1.

Figure S4, related to Figure 6

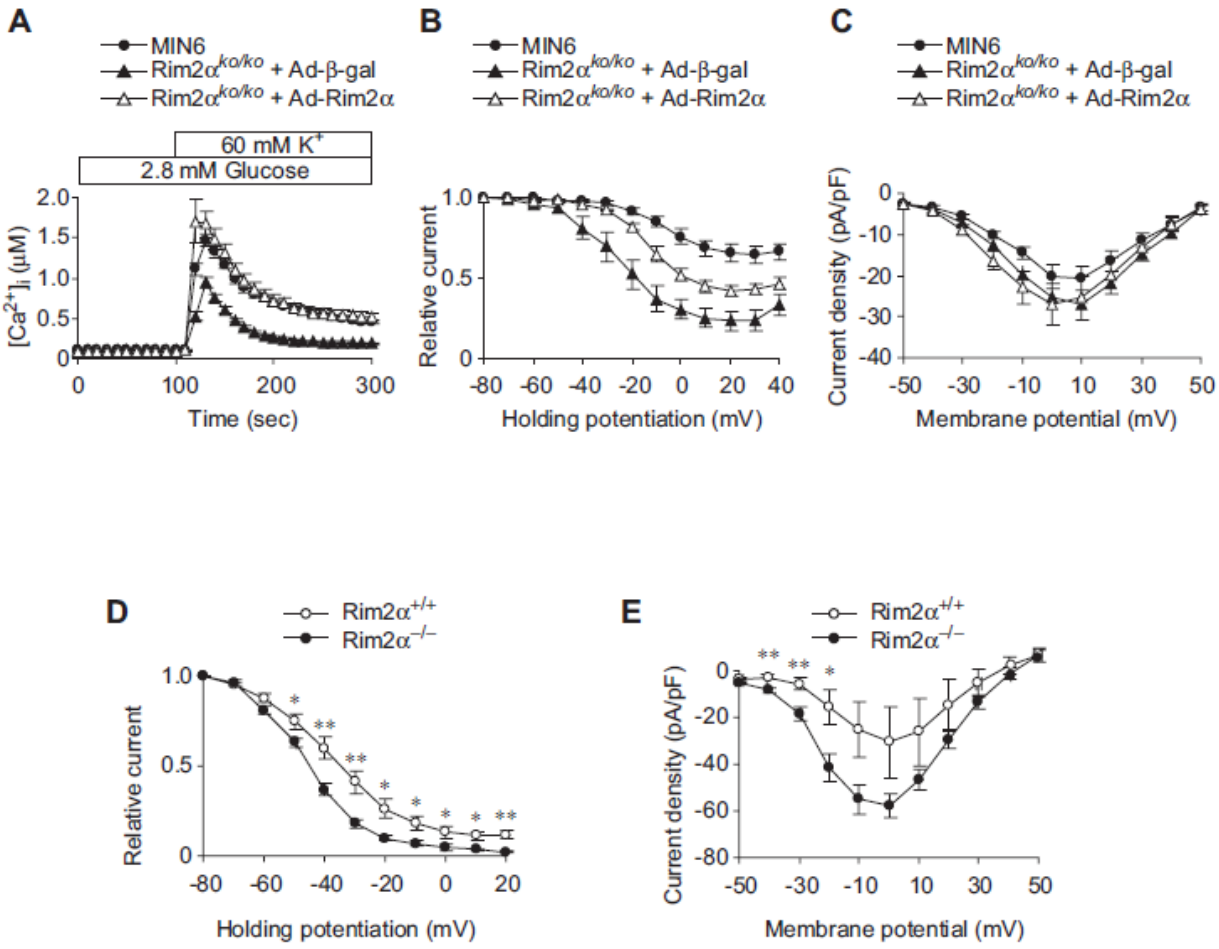

Figure S4. Effect of Rim2α in regulation of VDCC activity

(A) Effect of Rim2α on the intracellular Ca^{2+} concentration in Rim2α$^{ko/ko}$ β-cells. The intracellular Ca^{2+} concentration by depolarizing stimulation is significantly decreased in Rim2α$^{ko/ko}$ β-cells. When WT Rim2α was exogenously introduced, the decreased Ca^{2+} concentration is restored.

(B) Effect of Rim2α on inactivation curves of VDCC currents elicited in Rim2α$^{ko/ko}$ β-cells. To determine the voltage-dependence of inactivation (inactivation curve) of VDCCs, Ba^{2+} currents were evoked by 20-ms test pulse to 5 mV after the 10-ms repolarization to –80 mV following 2-s holding potential (V_h) displacement (conditioning pulse) from –80 mV to 40 mV in 10-mV increments. Amplitudes of currents elicited by the test pulses are normalized to those elicited by the test pulse after a conditioning pulse to –80 mV. The mean values were plotted against potentials of the conditioning

pulses. Inactivation is markedly accelerated in VDCC currents of Rim2α$^{ko/ko}$ β-cells. When WT Rim2α was introduced, the VDCCs show a depolarizing shift in voltage dependence of inactivation.

(C) Current density-voltage (*I-V*) relationships of VDCCs. To determine the *I-V* relationships, Ba^{2+} currents elicited by application of 30-ms test pluses from –50 mV to 50 mV in 10-mV increments from a V_h of –80 mV were analyzed. There are no statistical differences in *I-V* relationships between MIN6 cells and Rim2α$^{ko/ko}$ β-cells. Data were obtained from 3 independent experiments (n = 4-6) and expressed as means ± SEM.

(D) Effect of Rim2α on inactivation curves of VDCC currents elicited in β-cells isolated from Rim2α$^{-/-}$ mice. To determine the inactivation curve, Ba^{2+} currents were evoked by test pulse following conditioning pulse from –80 mV to 20 mV in 10-mV increments. Inactivation is markedly enhanced in VDCC currents of β-cells isolated from Rim2α$^{-/-}$ mice. Data were obtained from 2-3 independent experiments (n = 6-18) and expressed as means ± SEM.

(E) *I-V* relationships of VDCCs. To determine the *I-V* relationships, Ba^{2+} currents elicited by application of 30-ms test pluses from –50 mV to 40 mV in 10-mV increments from a V_h of –80 mV were analyzed. The VDCC inward currents of β-cells isolated from Rim2α$^{-/-}$ mice are larger than those of β-cells isolated from Rim2α$^{+/+}$ mice. Data were obtained from 2-3 independent experiments (n = 5-11) and expressed as means ± SEM. *$p < 0.05$, **$p < 0.01$ (Student's unpaired *t*-test).

Supplemental Experimental Procedures

Reagents

PMA was purchased from Sigma (St. Louis, MO). 8-pCPT-2'-*O*-Me-cAMP-AM was from BIOLOG (Bremen, Germany). Synthetic human GIP was from Peptide Institute (Osaka, Japan). Twinline enteral formula, which contains 17.0 kcal protein, 60.1 kcal carbohydrate, and 26.4 kcal fat/ 100 ml, was from Otsuka Pharmaceuticals (Tokushima, Japan). RNeasy Kit was from Qiagen, (Hilden, Germany). ReverTra Ace-α-Kit was from Toyobo (Osaka, Japan). SYBR Premix Ex Taq^{TM} was from Takara (Tokyo, Japan). Protease inhibitor cocktail was from Roche (Indianapolis, IN). Rabbit anti-Rim2, rabbit anti-Munc13-1, and rabbit anti-ELKS 1b/2 antibodies were from Synaptic systems (Göttingen, Germany). Mouse anti-Rab3, mouse anti-Chromogranin-A, mouse anti-Rab8, and mouse anti-Munc18 antibodies were from BD Transduction Laboratories (Lexington, KY). Rabbit anti-Syntaxin1 and mouse anti-glucagon antibodies were from Sigma (St. Louis, MO). Guinea pig anti-insulin antibody was from Zymed (San Francisco, CA). Mouse anti-Na^+-K^+-ATPase α-1 antibody was from Upstate Biotechnology (Lake Placid, NY). Rabbit anti-TFIID and mouse anti-Epac2 antibodies were from Santa Cruz Biotechnology (Santa Cruz, CA). Rabbit anti-Rab27A/B antibody was from Immuno-Biological Laboratories Co. (Gunma, Japan). Chicken anti-Liprin-α1 antibody was from Abcam (Tokyo, Japan). Alexa Fluor 488-conjugated goat anti-rabbit and anti-mouse IgG antibodies and Alexa Fluor 546-conjugated goat anti-guinea pig IgG antibody were from Invitrogen (Carlsbad, CA).

Generation of Rim2α$^{-/-}$ mice

Rim2α$^{-/-}$ mice were generated by replacing the amino acid coding sequences in exon 4 of mouse Rim2 with Neo cassette as described. The mice were backcrossed to mouse strain C57BL/6 at least over five generations. All animal procedures were approved by the Kobe University Animal Care Committee. PCR genotyping was performed on DNA extracted from tail biopsies using the following sets of primers: Neomycin (forward 5′-GATGGATTGCACGCAGGTTC and reverse 5′-CTTCCATCCGAGTACGTGCT) and Rim2α (forward 5′-CCAGCTATTGTCTATTGGCAT and reverse 5'-CTCCATTAGGCCAGTGTGAT).

Measurements of $[Ca^{2+}]_i$

Rim2α$^{ko/ko}$ β-cells were plated onto glass coverslips, and were infected with Ad-β-gal or Ad-Rim2α at a MOI of 1. After 48 h of infection, the cells on coverslips were loaded with 1 μM fura-2/AM (Dojindo

Laboratories, Kumamoto, Japan) in DMEM containing 10% fetal bovine serum at 37°C for 20 min, and washed with HEPES-KRB buffer containing 2.8 mM glucose. The coverslips were then plated in a chamber mounted on the stage of the microscopy. The cells were preincubated with HEPES-KRB buffer containing 2.8 mM glucose at 37°C for 30 min. One hundred seconds after acquisition of the image, the cells were stimulated with 60 mM K^+. Fluorescence images of the cells were recorded and analyzed with a video image analysis system (ARGUS CA-20 or AQUACOSMOS; Hamamatsu Photonics, Hamamatsu, Japan). All ratio data were calculated to $[Ca^{2+}]_i$ using an *in vitro* calibration method (Mori et al., 2002).

Current recordings

Whole-cell mode of the patch-clamp technique was carried out at 22–25°C with EPC-9 (HEKA Elektronik) and Axon 200B patch-clamp amplifiers (Molecular Devices) as previously described (Kiyonaka et al., 2007). Patch pipettes were made from borosilicate glass capillaries (1.5 mm outer diameter, 0.87 mm inner diameter; Hilgenberg) using a model P-87 Flaming-Brown micropipette puller (Sutter Instrument Co.). Pipette resistance ranged from 2 to 3.5 megohm when filled with the pipette solutions described below. The series resistance was electronically compensated to >60%, and both the leakage and the remaining capacitance were subtracted by –P/4 method. Currents were sampled at 20 kHz after low pass filtering at 3.0 kHz (3 db). An external solution contained (in mM): 10 $BaCl_2$, 153 tetraethylammonium chloride (TEA-Cl), 10 HEPES, and 10 glucose (pH 7.4 adjusted with TEA-OH). The pipette solution contained (in mM): 95 CsOH, 95 aspartate, 40 CsCl, 4 $MgCl_2$, 5 EGTA, 2 disodium ATP, 5 HEPES and 8 creatine phosphate (pH 7.2 adjusted with CsOH).

Supplemental References

Kiyonaka, S., Wakamori, M., Miki, T., Uriu, Y., Nonaka, M., Bito, H., Beedle, A. M., Mori, E., Hara, Y., De Waard, M., *et al.* (2007). RIM1 confers sustained activity and neurotransmitter vesicle anchoring to presynaptic Ca^{2+} channels. Nat. Neurosci. *10*, 691-701.

Mori, Y., Wakamori, M., Miyakawa, T., Hermosura, M., Hara, Y., Nishida, M., Hirose, K., Mizushima, A., Kurosaki, M., Mori, E., *et al.* (2002). Transient receptor potential 1 regulates capacitative Ca^{2+} entry and Ca^{2+} release from endoplasmic reticulum in B lymphocytes. J. Exp. Med. *195*, 673-681.